The Effects of Ocean Surface Waves on Global Intraseasonal Prediction: Case Studies with a Coupled CFSv2.0-WW3

Ruizi Shi[1], Fanghua Xu[1*], Li Liu[1], Zheng Fan[1], Hao Yu[1], Hong Li[1,3], Xiang Li[2] and Yunfei Zhang[2]

[1] Ministry of Education Key Laboratory for Earth System Modeling, and Department of Earth System Science, Tsinghua University, Beijing, 100084, China

[2] Key Laboratory of Marine Hazards Forecasting, National Marine Environmental Forecasting Center, Ministry of Natural Resources, Beijing, 100081, China

[3] Department of Atmospheric and Oceanic Sciences and Institute of Atmospheric Sciences, Fudan University, Shanghai, 200433, China.

**Correspondence to*: Fanghua Xu (fxu@mail.tsinghua.edu.cn)

Abstract. This ~~paper~~article describes the implementation of ~~evaluated~~ ~~Ocean surface gravity waves have enormous effects on physical processes at the atmosphere–ocean interface. t~~The effects of wave related processes on global intraseasonal prediction, by ~~were evaluated after we incorporating~~ed ~~a~~the coupling between~~WAVEWATCH III model~~ a global forecast ~~climate~~ model ~~into the Climate Forecast System model version 2.0~~ (CFSv2.0) and a wave model (WW3), and investigates the effects of ocean surface waves on air-sea interface in the new framework~~, with the Chinese Community Coupler version 2.0.~~. Several major wave-related processes, including the Langmuir mixing, Stokes-Coriolis force with entrainment, air-sea fluxes modified by Stokes drift and momentum roughness length, ~~were~~ are evaluated in two groups of 56-day experiments, one for boreal winter and the other for boreal summer. Comparisons ~~were~~ are ~~performed~~ made against in-situ buoys, satellite measurements and reanalysis data, to evaluate the influence of waves on intraseasonal prediction of sea surface temperature (SST), 2-m air temperature (T02), mixed layer depth (MLD), 10-m wind speed (WSP10) and significant wave height (SWH) ~~in CFSv2.0~~. The wave-coupled experiments show that o~~O~~verestimated SSTs and T02s, as well as underestimated MLDs at~~in~~ ~~mid and high~~mid-high latitudes in summer from original CFSv2.0 are significantly ~~clearly~~ improved~~, mainly~~ due to enhanced vertical mixing generated by Stokes drift. ~~The largest regional mean SST improvement reaches 35.89% in the Southern Ocean. of RMSE in austral summer~~For WSP10s and SWHs, the wave-related processes generally lead to reduction of biases in regions where WSP10s and SWHs are overestimated. On one hand, the decreased SSTs stabilize~~s~~ marine atmospheric boundary layer, weaken~~s~~ WSP10s~~wind speeds~~ and then SWHs. On the other hand, the increased roughness length due to waves leads to reduction in the originally overestimated WSP10s~~wind speed~~ and SWHs. In addition, the effects of Stokes drift and current on air-sea fluxes also rectify WSP10s and SWHs. ~~For WSP10 and SWH, the wave-related processes generally lead to reduction of biases in~~

~~regions where wind speed and SWH are overestimated. The decreased SST caused by Stokes drift related mixing stabilizes marine atmospheric boundary layer, weakens wind speed and then SWH. Compared with the NDBC buoy data, (1.24 m/s)()and the RMSEs of SWH decrease from ~~ ~~()(() the overestimated WSP10 is improved by up to 13.52% in boreal summer. The increased roughness length due to waves leads to some reduction in the originally overestimated wind speed and SWH, with the largest SWH improvement of 11.93% and 20.05% in boreal winter and summer respectively. The effects of Stokes drift and current on air sea fluxes are investigated separately. Their overall effects on air sea fluxes reduce the overestimated WSP10 by up to 17.31% and 23.21% in boreal winter and summer respectively.~~

These cases are helpful for the future development of the two-way CFSv2.0-wave coupled system.

1 Introduction

Ocean surface gravity waves play an important role in modifying physical processes at the atmosphere–ocean interface, which can influence momentum, heat and freshwater fluxes across the air-sea interface (Li and Garrett 1997; Taylor and Yelland, 2001; Moon et al., 2004; Janssen 2004; Belcher et al., 2012; Moum and Smyth, 2019). For instance, ocean surface waves modify ocean surface roughness to influence the marine atmospheric boundary layer and thus change the momentum, latent heat, and sensible heat transfer (Janssen 1989, 1991; Taylor and Yelland, 2001; Moon et al., 2004; Drennan et al., 2003, 2005). The breaking waves inject turbulent kinetic energy in the upper ocean, which enhances the mixing process (Terray et al. 1996). Nonbreaking surface waves also affect mixing in the upper ocean by adding a wave-related Reynolds stress (Qiao et al., 2004; Ghantous and Babanin, 2014). The wave-related Stokes drift interacts with Coriolis force and produces the Coriolis-Stokes force (Hasselmann 1970). The shear of Stokes drift is critical for generation of Langmuir circulation, which significantly deepens the mixed layer by strong vertical mixing both at climate scales (Li and Garrett 1997; Belcher et al., 2012) and at weather scales (Kukulka et al., 2009).

~~As Fox-Kemper et al. (2019) indicated, the improvement to atmosphere-ocean coupling with a better representation of the effects of surface gravity waves, is one of the challenges and focuses in ocean modeling for the next decade. Regional coupled models, such as the well-known Coupled Ocean-Atmosphere-Wave-Sediment Transport Modeling System (COAWST; Warner et al., 2010), were developed to study tropical cyclones, storm surge and other coastal processes at small or meso-scales (e.g., Prakash et al., 2018; Ricchi et al., 2017; Pianezze et al., 2018; Wu Sun et al., 2019). The Coupled~~

~~Ocean-Atmosphere-Wave-Sediment-Transport-Modeling-System-(COAWST)-developed-by-Warner-et al.-(2010)-is-one-of-the-well-known-fully-coupled-regional-models,-which-has-been-applied-in-various locations-such-as-the-South-China-Sea-(Sun-et-al.,-2019;-Wu-et-al.,-2019),-the-Bay-of-Bengal-(Prakash-et al.,-2018)-and-the-Mediterranean-Sea-(Ricchi-et-al.,-2017).-On-the-other-hand,-most-of-the-coupled-models with-a-wave-component-at-global-scale-were-developed-for-climate-research-(e.g.,-Qiao-et-al.,-2010;-Law-Chune-and-Aouf,-2018;-Fan-et-al.,-2012;-Fan-and-Griffies,-2014;-Li-et-al.-2016,-2017).-Exceptionally,-an Integrated-Forecasting-System-(IFS)-with-fully-coupled-atmosphere,-ocean-and-wave-components, developed-by-European-Centre-for-Medium-Range-Weather-Forecasts-(ECMWF)-(Janssen-2004;-Bidlot et-al.-2019,-2020),-has-been-released-with-great-flexibility-for-global-forecasts-from-medium-range weather-scales-to-seasonal-scales-(Breivik-et-al.-2015).~~

~~The overall effects of wave-related processes have been shown to be important in global coupled systems for both climate research (e.g., Law-Chune and Aouf, 2018; Bao et al. 2019; Couvelard et al. 2020) and numerical prediction (Breivik et al. 2015; Bidlot et al. 2019, 2020)~~~~The overall effects of wave-related processes on numerical prediction have been shown to be important in coupled systems (e.g., Law-Chune and Aouf, 2018; Bao et al. 2019; Couvelard et al. 2020).~~ For instance, das well as subsurface ~~temperature sNucleus for European Modelling of the Ocean (NEMO) with wind input and wave dissipationand the with misalignment of winds and wavesoceanic surface momentum fluxreducemixed layer depth (MLD)biases in NEMO~~

Various ~~The contribution of individual w~~wave-related ~~process, howev~~parameterizations have been proposed and applied in modeling~~er, is complex and studied severally~~individually ~~(e.g. Janssen 2004; Breivik et al. 2015; Janssen and Bidlot 2018; Pineau-Guillou et al. 2018).~~ ~~As long been recognized,~~

~~waves play an important role in directly interactions with winds (Janssen 2004; Janssen and Bidlot 2018).~~ ~~For instance,~~ T~~t~~he wave-related Charnock parameter (C_{ch}) ~~changes~~defines sea surface roughness and affects ~~to modify~~ wind stress estimates~~, and then corrects simulated wind speed~~ (Pineau-Guillou et al. 2018; Sauvage et al. 2020). There are primarily three methods for C_{ch}, assessed from the wave-induced kinematic stress (Janssen 1989, 1991), the wave age (Drennan et al., 2003, 2005; Moon et al., 2004~~; Fan et al. 2012~~), or the steepness (Taylor and Yelland, 2001). The former two are based on the wind-sea conditions, whereas the latter includes both swells and wind-sea waves. ~~To better fit the observed leveling off roughness length for high winds, several modifications were conducted, such as a simply limit for the maximum roughness (WAVEWATCH III Development Group, 2016) or M~~modifications to ~~regular~~these Charnock parameterizations were suggested in recent studies for the leveling off roughness under high winds (e.g. Fan et al., 2012; Bidlot et al., 2020; ECMWF, 2020; Li et al., 2021). ~~In addition,~~ In the oceanic boundary layer, waves ~~also~~ influence upper ocean mixing via wave dissipation and Stokes drift-induced ~~Langmuir cells~~processes. In Breivik et al. (2015), the wave dissipation-related turbulent kinetic energy flux is found to yield the largest sea surface temperature (SST) differences in the extratropics. The Stokes drift-induced ~~Stokes drift related~~ Langmuir ~~cell~~turbulence ~~was demonstrated to enable~~can improve~~ments of simulated~~ temperature ~~structure~~ simulation ~~in the upper ocean~~ over most of the world oceans, particularly in the Southern Ocean (Belcher et al., 2012; Li et al., 2016). Polonichko (1997), Van Roekel et al. (2012) and Li et al. (2017) ~~and Van Roekel et al. (2012)~~ indicated that ~~Because t~~the Langmuir cell intensity strongly depends on the alignment of~~depends on the misalignment of~~ winds and waves ~~(Polonichko, 1997; Van Roekel et al., 2012),~~ reaching maximum when they are aligned. Li et al. (2016) found the effect of Langmuir cell c~~ould~~an be further enhanced ~~due to~~by entrainment ~~(Li et al., 2016)~~. In Couvelard et al. (2020), the Stokes drift–related force~~t~~ can also

contributes to modest deepening of the mixed layer depth (MLD) modestly(Couvelard et al., 2020).In ,the is found to yield the largest differences in NEMO. Stokes… Besides, the Stokes drift play a role in the relative velocity determined turbulent fluxes In the First Institute of Oceanography Earth System Model, (Bao et al. (2019) indicated that the non-breaking waved-induced mixing, Stokes drifts affected air-sea fluxes, as well as sea spray are all important for climate estimates. .

,

The wave-related processes at the air-sea interface are complex and important in global coupled systems (e.g., Breivik et al. 2015; Law-Chune and Aouf, 2018; Bao et al. 2019; Bidlot et al. 2019, 2020; Couvelard et al. 2020). Most of the coupled models with a wave component at global scale were developed for climate research (e.g., Qiao et al., 2010; Law-Chune and Aouf, 2018; Bao et al. 2019; Couvelard et al. 2020 Fan et al., 2012; Fan and Griffies, 2014; Li et al. 2016, 2017). Exceptionally, an Integrated Forecasting System (IFS) with fully coupled atmosphere, ocean and wave components, developed by European Centre for Medium-Range Weather Forecasts (ECMWF) (Janssen 2004; Bidlot et al. 2019, 2020), has been released with great flexibility for global forecasts from medium-range weather scales to seasonal scales (Breivik et al. 2015).

The effects of wave-related processes are worth further evaluation in different global coupled modelling systems. The wave related processes are worth and worth further evaluation in different modelling systems. Since it takes sufficient periods for the wave energy to develop (Janssen 2004), it is of great interest to we investigate the impact of individual wave process effect at intraseasonal timescale in a new global atmosphere-ocean-wave system. Several wave related processes are studied, including upper ocean mixing modified by Langmuir cell, Stokes-Coriolis force and entrainment, air-sea fluxes modified by surface current and Stokes drift, and momentum roughness length. All these processes

~~greatly affect momentum and enthalpy fluxes across the air-sea interface (e.g., Fan et al., 2012; Fan and Griffies, 2014; Li et al. 2016, 2017; Renault et al. 2012; Varlas et al. 2020).~~To achieve this, we coupled the WAVEWATCH III (WW3) to the Climate Forecast System model version 2.0 (CFSv2.0) and then conducted sensitivity experiments in boreal winter and summer for comparison. The effects of upper ocean mixing modified by Langmuir cell, Stokes-Coriolis force and entrainment, air-sea fluxes modified by surface current and Stokes drift, and momentum roughness length are evaluated. The CFSv2.0 is a coupled system with main application for intraseasonal and seasonal prediction (e.g. Saha et al. 2014). The National Centers for Environmental Prediction (NCEP) is establishing its own atmosphere-ocean-wave system, in which the Global Forecast System (GFS; the atmosphere module in CFSv2.0 system) is one-way coupled with WW3. Our work can provide insights for two-way wave coupling of CFSv2.0, and is helpful for the future development of the CFSv2.0-wave coupling system.

~~Several wave-related processes are studied, including upper-ocean mixing modified by Langmuir cell, Stokes-Coriolis force and entrainment, air-sea fluxes modified by surface current and Stokes drift, and momentum roughness length. All these processes greatly affect momentum and enthalpy fluxes across the air-sea interface (e.g., Fan et al., 2012; Fan and Griffies, 2014; Li et al. 2016, 2017; Renault et al. 2012; Varlas et al. 2020).~~ Two groups of 56-day predictions were conducted for boreal winter and boreal summer, respectively. The predictions were then compared with observations and reanalysis data. For each group, sensitivity experiments with different wave parameterizations were carried out to evaluate the effects of individual wave-related process.

The rest of the paper is structured as follows: methods and numerical experiments with different parameterizations are described in Section 2; the observations and reanalysis data are introduced in Section 3, and the results of experiments are evaluated and compared in Section 4. Finally, a summary

and discussion are given in Section 5.

2 Methods and Experiments

2.1 Coupling WAVEWATCH III with CFSv2.0

The version 5.16 of WW3 (WAVEWATCH III Development Group, 2016) developed by the National Oceanic and Atmospheric Administration (NOAA)/NCEP has been incorporated into the CFSv2.0 (Saha et al., 2014) as a new model component. The latitude range of WW3 is 78°S–78°N with a spatial resolution of 1/3°; the frequency range is 0.04118-0.4056Hz and the total number of frequencies is 25; the number of wave directions is 24 with a resolution of 15°; the maximum global time step and the minimum source term time step are both 180 s.

The CFSv2.0 contains two components, the GFS (details are available at http://www.emc.ncep.noaa.gov/GFS/doc.php) as the atmosphere component and the Modular Ocean Model version 4 (MOM4; Griffies et al., 2004) as the ocean component. The MOM4 is integrated on a nominal 0.5° horizontal grid with enhanced horizontal resolution to 0.25° in the tropics, and has 40 vertical levels; the vertical spacing is 10 m in the upper 225 m, and then increases in unequal intervals to the bottom at 4478.5 m. A three-layer sea ice model is included in MOM4 (Wu et al. 2005). The GFS uses a spectral triangular truncation of 382 waves (T382) in the horizontal, which is equivalent to a grid resolution of nearly 35 km, and 64 sigma-pressure hybrid layers in the vertical. ~~The CFSv2.0 uses a~~A ~~two-layer Sea Ice Model (SIM) is applied in CFSv2.0 (Wu et al. 2005).~~ The time steps of both MOM4 and GFS are 180 s. The ocean and atmosphere components are then coupled at the same rate. In the original two-way coupled system, the GFS receives SST from MOM4 and sends fluxes of heat, momentum, freshwater to MOM4 (black arrows in Fig. 1). ~~The CFSv2.0 uses a two-layer Sea Ice Model~~

~~(Wu et al. 2005)~~

The Chinese Community Coupler version 2.0 (C-Coupler2; Liu et al., 2018) is applied to interpolate and pass variables between atmosphere and wave components as well as ocean and wave components. Each component receives inputs and supplies outputs on its own grids. The C-Coupler2 is a common, flexible and user-friendly coupler, which contains a dynamic 3-D coupling system and enables variables to remain conserved after interpolation. ~~From a series of tests of coupling experiments, the time step of wave coupling (1800 s) was selected to compromise time consumption and model bias (details in Table S1 of the supplementary). To quantify the sensitivity of coupling frequency, the root mean square errors (RMSEs) of SST, significant wave height (SWH) and 10 m wind speed (WSP10) with different coupling steps for the fully coupled experiment (ALL; details in Section 2.6) are shown in Table S1 of the supplementary. From Table S1, the 10_STEP_WW3 experiment has the closest RMSEs to the 1_STEP_ALL for SST, SWH and WSP10, and has the relatively small runtime. Therefore, the time steps of 10_STEP_WW3 are selected to compromise computer time consumption and the model RMSE.~~

A schematic diagram of the coupled atmosphere-ocean-wave system is shown in Fig. 1. As illustrated, WW3 is two-way coupled with MOM4 and GFS, through the C-Coupler2. WW3 is forced by 10-m wind from GFS (green arrows) and surface current from MOM4 (blue arrows), and then generates and evolves the wave action density spectrum. Meanwhile, the surface Stokes drift velocity, the Stokes transport ~~with~~ and the turbulent Langmuir number ~~is~~ are passed to MOM4 (red arrows; see Section 2.3) from WW3, and the surface Stokes drift velocity and the Charnock parameter are passed to GFS (red arrows; see Section 2.4 and 2.5). The high frequency tail assumption for Stokes drift in WW3 is used with a spectral level decaying as f^{-5} (frequency). Additionally, the regular ocean surface current velocities from MOM4 are also passed to GFS, to ~~estimate~~calculate the relative wind velocity for the turbulent fluxes together

with surface Stokes drift (blue arrows; see Section 2.4).

~~In this study, b~~Both the CFSv2.0 and WW3 use warm starts; the ~~daily~~ initial fields at 00:00 UTC of the first day in each experiment for CFSv2.0 were generated by the real time operational Climate Data Assimilation System (Kalnay et al., 1996), downloaded from the CFSv2.0 official website (http://nomads.ncep.noaa.gov/pub/data/nccf/com/cfs/prod). To get initial conditions for WW3, a stand-alone WW3 model is set up synchronously (see Section 2.2). Since the interactions between waves and sea ice are ~~too~~ complicated and beyond~~, which is outside our~~ the scope of the study, we ~~do not include an explicit coupling between waves and sea ice and~~ turn off the coupling between~~from~~ WW3 and~~to~~ CFSv2.0 in areas with sea ice. ~~The ice blocking IC0 source term with the critical ice concentration of 50% is applied. to avoid any conflicts with sea ice.when the critical sea ice concentration is reached.~~

In addition, to properly select the coupling frequency between CFSv2.0 and WW3, the root mean square errors (RMSEs) of SST, significant wave height (SWH) and 10-m wind speed (WSP10) with different coupling steps for the fully coupled experiment (ALL; details in Section 2.6) are calculated and compared (Table S1 of the supplementary). From Table S1, the 10_STEP_WW3 experiment has a relatively short runtime and small RMSEs. Therefore, the time steps of the 10_STEP_WW3 are selected to compromise computing time consumption and ~~the~~ model RMSEs.

2.2 Initialization of WAVEWATCH III

In WW3, input of momentum and energy by wind, and dissipation for wave-ocean interaction are two important terms (combined as input-dissipation source term) in the energy balance equation (WAVEWATCH III Development Group, 2016), which include the Charnock parameter related estimation. Several different packages to calculate the input-dissipation source term (ST) are offered in

the WW3 version 5.16, including ST2 (Tolman and Chalikov, 1996), ST3 (Janssen, 2004; Bidlot, 2012), ST4 (Ardhuin et al., 2010), and ST6 (Zieger et al., 2015).

The initial wave fields were generated from 10-day simulation starting from rest in a stand-alone WW3 model. To minimize the biases of initial wave fields, we tested simulations with ST2, ST3, ST4, and ST6 schemes respectively, and compared the results with Janson-3 observations. Two 10-m wind datasets, the Cross-Calibrated Multi-Platform (CCMP; Atlas et al., 2011) data and the fifth generation European Centre for Medium-Range Weather Forecasts (ECMWF) Reanalysis (ERA5; Hersbach et al., 2020) data, were used to drive the wave model respectively. Compared all results, the ST4 scheme with ERA5 wind forcing generates the minimum ~~significant wave height (~~SWH~~)~~ bias (Table S2 in the supplementary), consistent with findings in Stopa et al. (2016). Thus, the ST4 scheme was chosen to calculate the input and dissipation term, and generate initial wave fields with ERA5 wind forcing for experiments listed in Table 1. The parameters used for ST4 scheme followed TEST471f from WAVEWATCH III Development Group (2016), which is the CFSR (CFS Reanalysis) tuned setup and is commonly-used at global scale.

2.3 Parameterizations of Stokes Drift-Related Ocean Mixing

The full Stokes drift profile used in MOM4 is obtained by the method of Couvelard et al. (2020), which is based on the work of Breivik et al. (2014; 2016). Breivik et al. (2016) derived the full Stokes drift profile as

$$u_s B16(z) = u_s(0)[\exp(2k_p z) - \sqrt{-2\pi k_p z}\,\mathrm{erfc}(\sqrt{-2k_p z})], \quad (1)$$

The $u_s(0)$ is the surface Stokes drift velocity, $k_p = \frac{u_s(0)}{6V_s}$, V_s is the Stokes transport, and erfc is the complementary error function. ~~Considering the numerical models represent vertical and horizontal~~

averages over each grid box (Li et al., 2017; Wu et al., 2019; Couvelard et al., 2020). Eqn. 1 is depth-averaged within each vertical grid interval as,a finite volume approach should be added as

$$u_s(z) = \frac{u_s(0)}{(th)_k}[I(z_{k+1/2}, k_p) - I(z_{k-1/2}, k_p)], \quad (2)$$

$$I(z, k_p) = \frac{1}{6k_p}[e^{2k_p z} + 4k_p z\frac{u_s B16(z)}{u_s(0)}], \quad (3)$$

where *th* is the thickness of layer *k*, following Li et al., (2017), Wu et al., (2019) and Couvelard et al., (2020). Besides, the vertical component of Stokes drift is diagnosed from the continuity equation.

2.3.1 Mixing of Langmuir Turbulence

McWilliams and Sullivan (2000) modified the turbulent velocity scale W in K-Pprofile Pparameterization (KPP) for vertical mixing by introducing an enhancement factor ε, to account for both boundary layer depth changes and nonlocal mixing by Langmuir turbulence. Based on their work, VanVan Roekel et al. (2012) improved the enhancement factor corresponding to alignment and misalignment of winds and waves. Li et al. (2016) evaluated these parameterizations in a coupled global climate model, and found that the difference between parameterizations with alignment and with misalignment was not significant, owing to the relatively coarse resolution which cannot accurately represent the refraction by coasts and current features., and parameterizations from VanVan Roekel et al. (2012) showed best performance. However, the difference between parameterizations with alignment and misalignment was not significant, owing to the coarse resolution which cannot accurately represent the refraction by coasts and current features. Besides, the misalignment will certainly increase the runtime due to increased variables to be transferred from wave to ocean. Hence,Here wWe employed applied the parameterization corresponding to alignment of winds and waves from VanVan Roekel et al. (2012) as well. Because the mode resolution in our model is relatively coarse too, and As shown in Fig.

~~S1i&j in supplementary,~~ the angles between winds and waves are less than 30° in most areas (Fig. S1i&j in the supplementary),~~.~~ ~~In Li et al. (2016), the difference between parameterizations with alignment and misalignment was not significant, owing to the coarse resolution which cannot accurately represent the refraction by coasts and current features.~~ ~~Note~~Although~~the Langmuir cell intensity partly depends on the misalignment (Polonichko, 1997; Van Roekel et al., 2012), and assuming alignment of wind and waves leads to excessive mixing(,Since the misalignment between the Stokes drift and wind direction is important for the intensity of Langmuir cell (Polonichko, 1997; Van Roekel et al., 2012; Li et al., 2017), particularly in the Southern Ocean (Couvelard et al., 2020), the effects of the Stokes drift might be overestimated in this system.~~ ~~Without the misalignment, since the simulation still underestimated the mixing,~~ we didn't consider misalignment in the study.~~.~~ ~~Since the misalignment between the Stokes drift and wind direction is important for the intensity of Langmuir cell (Polonichko, 1997; Van Roekel et al., 2012; Li et al., 2017), particularly in the Southern Ocean (Couvelard et al., 2020), the effects of the Stokes drift might be overestimated in this system.~~

~~*In the study,*~~ *W* (*W*=ku_*/ϕ, where u_* is the surface friction velocity, ϕ is the dimensionless flux profile, and *k*=0.4 is the von Kármán constant) varies in proportion to the turbulent Langmuir number, that is,

$$\mathrm{W} = \frac{ku_*}{\phi}\varepsilon, \qquad (\sim\!\!4)$$

$$\varepsilon = \sqrt{1 + (3.1La_\mathrm{t})^{-2} + (5.4La_\mathrm{t})^{-4}}, \qquad (\sim\!\!5)$$

where La_t is the turbulent Langmuir number, defined as

$$La_\mathrm{t} = \sqrt{\frac{u_*}{|u_s(0)|}}, \qquad (\sim\!\!6)$$

with $u_s(0)$ is the surface Stokes drift velocity.

Furthermore, the enhanced W will influence the calculation of boundary layer depth. In KPP the boundary layer depth is determined as the smallest depth at which the bulk Richardson number equals the critical value $Ri_{\mathrm{cr}} = 0.3$, that is,

$$Ri_b(h) = \frac{gh[\rho_r - \rho(h)]}{\rho_0[|u_r - u(h)|^2 + W^2]} = Ri_{\mathrm{cr}}, \quad (47)$$

where g is acceleration of gravity, ρ is density, u is velocity, ρ_r is surface density, u_r is surface velocity, ρ_0 is an average value and h is the boundary layer depth. Hence, when W is enhanced, the boundary layer depth h is deepened accordingly.

2.3.2 Stokes–Coriolis Force and Associated Entrainment

Because the Stokes drift velocity is an increment superimposed on the original current velocity, the Coriolis force and the Stoke drift together produce an additional so-called Stokes–Coriolis (SC) force (Hasselmann 1970), that is,

$$SC\ Force = \overrightarrow{\mathrm{u_s(z)}\cancel{u_s}} \times f\vec{z}. \quad (\cancel{5}8)$$

Here $\overrightarrow{\mathrm{u_s(z)}\cancel{u_s}}$ is ~~surface~~ the Stokes drift velocity vector, f is the Coriolis frequency, and $\vec{z}$ is the vertical unity vector. For consistency~~geostrophic~~, the Stokes drift velocity ~~vector~~ is also ~~considered~~included in advection terms of tracers (e.g. temperature, salinity) and convergence terms (Law-Chune and Aouf, 2018; Couvelard et al., 2020~~references??~~). And the free surface condition for barotropic mode is correspondingly modified to

$$\frac{\partial \eta}{\partial t} = -\nabla \mathrm{M_{curr}} - \nabla \mathrm{M_{st}}, \quad (9)$$

where η is surface elevation, $\mathrm{M_{curr}}$ and $\mathrm{M_{st}}$ are the total vertical integral of regular Eulerian current and Stokes drift, respectively.

To depict the entrainment below the ocean surface boundary layer induced by Stokes drift, Li et al.

(2016) suggested to add the square of surface Stokes drift velocity ($|u_s(0)|^2$) to the denominator of Eqn. 47, that is,

$$Ri_b(h) = \frac{gh[\rho_r - \rho(h)]}{\rho_0[|u_r - u(h)|^2 + W^2 + |u_s(0)|^2]} = Ri_{\mathrm{cr}}. \quad (6\,10)$$

The boundary layer depth h in KPP from Eqn. 6 10 is then enhanced due to Stokes drift velocity.

2.4 Stokes Drift and Sea Surface Current on Air–Sea Fluxes

At air-sea boundary layer, the momentum flux (τ), sensible heat flux (SH) and freshwater flux (E) are calculated as

$$\tau = \rho_a C_d |\Delta\vec{V}|\Delta\vec{V}, \quad (7\,11)$$

$$SH = \rho_a C_h |\Delta\vec{V}|\Delta\theta, \quad (8\,12)$$

$$E = \rho_a C_e |\Delta\vec{V}|\Delta q, \quad (9\,13)$$

where C_d, C_h, C_e are surface exchange coefficients for momentum, sensible heat and freshwater. ρ_a is air density. $\Delta\theta, \Delta q$ are potential temperature and humidity differences between air and sea, and $\Delta\vec{V}$ is velocity of air relative to water flow.

In CFSv2.0, $\Delta\vec{V}$ is set to be wind speed ($\overrightarrow{U_{wind}}$). However, the effect of ocean surface current should not be ignored. Luo et al. (2005) first indicated that including ocean surface current ($\overrightarrow{U_{surf}}$) improves estimates of τ and subsequent ocean response. Renault et al. (2016) further indicated that the improvements of τ by $\overrightarrow{U_{surf}}$ also feed back into atmosphere. At present, $\Delta\vec{V} = \overrightarrow{U_{wind}} - \overrightarrow{U_{surf}}$ is widely used in coupled ocean-atmosphere models (e.g., Hersbach and Bidlot, 2008; Takatama et al., 2017; Renault et al., 2021). Furthermore, Bao et al. (2019) indicated that as a part of the sea surface water movement with speed magnitude comparable to surface current in mid-high latitudes, the surface Stokes drift ($\overrightarrow{u_s(0)}$) should also be included, that is,

$$\Delta\vec{V} = \overrightarrow{U_{wind}} - \overrightarrow{U_{surf}} - \overrightarrow{u_s(0)}. \quad (10\,14)$$

To account for the effects of Stokes drift velocity, the Eqn. 10 14 was applied in the coupled experiments (Table 1), and the difference compared with $\Delta\vec{V} = \overrightarrow{U_{wind}} - \overrightarrow{U_{surf}}$ was analyzed in Section 4.4. To complete the coupling, the corresponding modification of the tridiagonal matrix (Lemarié 2015) is also conducted in CFSv2.0. Note that the direction of Stokes drift is generally consistent with 10-m wind (Fig. S1a, b, e, fi&j in supplementary), but the directions of surface current and 10-m wind are usually with an angle due to Coriolis effect (Fig. S1a dg&h). Consequently, the effects of $\overrightarrow{U_{surf}}$ and $\overrightarrow{u_s(0)}$ on $\Delta\vec{V}$ depend on the angles between them and $\overrightarrow{U_{wind}}$.

2.5 Parameterizations of Momentum Roughness

In CFSv2.0, the fluxes of momentum, heat, and freshwater are passed from atmosphere to ocean, and the estimates of them are critically important. The fluxes are in part determined by surface roughness length, which can be converted to surface exchange coefficients in Eqn. 11-13 7-9.

2.5.1 The Momentum Roughness Length in GFS

In GFS, the momentum roughness length z_0 has two terms. The first term z_{ch} is parameterized by the Charnock relationship (Charnock, 1955) representing wave-resulted sea surface roughness, and the second term z_{vis} is the viscous contribution (Beljaars, 1994) for low winds and smooth surface, that is,

$$z_0 = z_{ch} + z_{vis} = \frac{C_{ch}u_*^2}{g} + \frac{0.11\nu}{u_*}. \quad (11\,15)$$

Here $C_{ch} = 0.014$ is the constant Charnock parameter, ν is the air kinematic viscosity. The relation of z_0 in GFS versus 10-m wind speed is shown in Fig.2 (black line).

2.5.2 The Charnock Relationship Related to Wave State

When ocean surface waves are explicitly considered, the Charnock parameter C_{ch} is not a constant (Janssen 1989, 1991; Taylor and Yelland, 2001; Moon et al., 2004; Drennan et al., 2003, 2005). ~~There are primarily three methods for C_{ch}, assessed from the wave induced kinematic stress (Janssen 1989, 1991), the wave age (Drennan et al., 2003, 2005; Moon et al., 2004; Fan et al., 2012), or the steepness (Taylor and Yelland, 2001). The former two are based on the wind sea conditions, whereas the latter includes both swells and wind-sea waves.~~ In the study, we adopted a method developed by Moon et al. (2004)~~Fan et al. (2012)~~, which considered the surface roughness leveling off under extremely high wind speed ~~based on the researches of~~ (Powell et al., ~~(~~2003~~),~~ ; Donelan et al. ~~(~~, 2004~~)~~, ~~and Moon et al. (2004)~~. Based on observations, Moon et al. (2004) proposed Eqn. 16 to estimate the Charnock parameter by the wave age $\frac{c_{pi}}{u_*}$ (c_{pi} is the peak phase speed of the dominant wind-forced waves) with~~, and gave~~ constant ~~different~~ values of a and b changing with 10-m wind speed every 5 m/s in the range~~ing~~ of ~~from~~ 10 m/s to 50 m/s. ~~In the parameterization, C_{ch} is calculated by the wave age $\frac{c_{pi}}{u_*}$ (c_{pi} is the peak phase speed of the dominant wind-forced waves) as~~

$$C_{ch} = a\left(\frac{c_{pi}}{u_*}\right)^b, \qquad (~~12~~16)$$

~~$$a = \frac{0.023}{1.0568^{U_{10}}}, b = 0.012U_{10}, \qquad (13)$$~~

~~where U_{10} is the 10-m wind speed.~~ To obtain continuous values of a and b, w~~W~~e derive a new~~the~~ relationship (Eqn. 17) ~~between~~ to estimate a and b~~a/b~~ ~~and~~from 10-m wind speed U_{10} by fitting the values in Table 1 of Moon et al. (2004) ~~for U_{10}>15 m/s,~~

$$a = \frac{1}{0.1477{U_{10}}^2 - 0.7395U_{10} - 10.9995},$$
$$b = 1.5661E^{-5}{U_{10}}^3 - 0.002{U_{10}}^2 + 0.1017U_{10} - 1.6182. \qquad (17)$$

Because the observations in Moon et al. (2004) were obtained under tropical cyclones, ~~there was no reliable data for wind ≤ 15 m/s. So,~~ Eqn. 17 is used for U_{10}>15 m/s, whereas the original Charnock relationship of WW3 ST4 scheme (Janssen 1989, 1991) is used for $U_{10} \leq$15 m/s. The revised parameterization is called ST4-M04. Figure S2 in supplementary shows the C_{ch} distribution obtained by Eqn. 1~~2 13~~6-17. In general s~~S~~mall wind direction variations at low latitudes lead to large wave age and thus ~~high~~ low C_{ch}~~, and vice versa~~. The situation is opposite at mid-high latitudes. ~~At mid-high latitudes C_{ch} is higher in summer winter than in wintersummer. (references??) ;~~

The relationships between z_0 and U_{10} in GFS, WW3 ST4 scheme (Janssen 1989, 1991) and ST4-~~FAN~~ M04 scheme ~~(Fan et al., 2012)~~ were compared in Fig.2. The z_0 in GFS increases relatively slowly with increasing wind speed (black). The value of z_0 from ST4 scheme (purple) increases rapidly with wind speed at high winds. In comparison, in ST4-~~FAN~~ M04 scheme (~~dark red~~blue) the rapid increase of z_0 at high wind speed is obviously restrained, although the mean z_0 is slightly higher than that in GFS ~~especially~~ at wind speed >10 m/s due to larger C_{ch} (>0.014 in Fig. S2). Furthermore, since the Charnock number is constant in GFS, the standard deviation (STD) of z_0 at a given wind speed is near zero. Since the z_0 is determined only by wind-sea conditions in ST4 and ST4-~~FAN~~ M04 scheme, the STD at a given wind speed is mainly owing to variations in wind fetch and development stage of sea state~~(Shimura et al., 2017)~~. The reduced STDs in ~~ST4-FAN~~ST4-M04 scheme, compared to ST4, imply less sensitivity of z_0 to fetch and sea state. Note that the ST4-M04 is used in GFS, while the z_0 in WW3 is still calculated by the ST4 source term to avoid affecting the balance ~~between~~of adjusted wind input and dissipation.

2.6 Set of Experiments

A series of numerical experiments was conducted to evaluate the effects of aforementioned wave-related processes on ocean and atmosphere in two 56-day periods, from January 3 to February 28, 2017 and from August 3 to September 28, 2018 for boreal winter and boreal summer, respectively.

The reference experiment (CTRL) is a one-way coupled experiment, in which CFSv2.0 provides 10-m wind and surface current to WW3, whereas no variable is transferred from WW3 to CFSv2.0. The results of CFSv2.0 in CTRL are consistent with the corresponding CFS Reanalysis data (Saha et al., 2010). For each period, four sensitivity experiments were carried out (Table 1). Based on CTRL, the first is VR12-AL-SC-EN experiment, in which the Langmuir mixing parameterization is applied with Stokes–Coriolis force and entrainment in MOM4. The second is Z0-M04 experiment, in which the constant C_{ch} in GFS is replaced by C_{ch} from WW3 ST4-M04 scheme. The effect of fluxes in GFS generated by $\Delta\vec{V}$ (Eqn. 14) is tested in the FLUX experiment. The last experiment is the ALL, which includes all three parameterizations.

3 Data

Due to the availability of in situ and reanalysis data in the simulation periods, only sea surface temperature (SST), ocean subsurface temperature and salinity (T/S), 2-m air temperature (T02), 10-m wind speed (WSP10), and significant wave height (SWH) were used to evaluate the simulation results.

The daily average satellite Optimum Interpolation SST (OISST) data were obtained from NOAA, with $0.25° \times 0.25°$ resolution (Reynolds et al., 2007; https://www.ncdc.noaa.gov/oisst). The global Argo observational profiles of T/S (Li et al., 2019) were from China Argo Real-time Data Center (www.argo.org.cn). The ERA5 datasets of T02, WSP10 and SWH with a spatial resolution of 0.5° were

also used (Hersbach et al., 2020; https://cds.climate.copernicus.eu/cdsapp#!/dataset/reanalysis-era5-single-levels), which assimilated huge amounts of historical data and thus provided reliable hourly estimates. Additionally, the WSP10 and SWH observations from the available National Data Buoy Center (NDBC) buoy data (https://www.ndbc.noaa.gov) were applied for comparison.

4 Experimental Results

In this section, an evaluation of simulation results was presented. Comparisons were made between model results and observations/reanalysis data. The results in the first three days were excluded in the evaluation, since the initial wave influences were too weak.

4.1 Sea Surface Temperature (SST) and 2-m Air Temperature (T02)

Figure 3a ~~and Figure 4a~~ shows the spatial distribution of 53-day (day 4 to day 56) averaged SST biases in CTRL in boreal winter ~~and summer, respectively.~~ ~~Here the bias in Fig.3a&4a is~~ defined as SST in CTRL minus OISST. ~~To highlight t~~The ~~differences of the other four experiments (Table 1) versus the CTRL are, a percentage relative difference (PRD) of the bias is computed~~ shown as ~~PRD = $\frac{|\widehat{y_s}-y|-|\widehat{y_c}-y|}{|y|} \times 100\%$, where y is OISST, $\widehat{y_c}$ is simulated SST in CTRL and $\widehat{y_s}$ is simulated SST in other experiments in (Fig. 3c-f and Fig. 4c-f (results of other four experiments minus CTRL)). The correlations between the absolute CTRL biases and the differences of absolute biases between ALL and CTRL ($|\widehat{y_a}-y|-|\widehat{y_c}-y|$, where y is OISST or ERA5, $\widehat{y_c}$ ($\widehat{y_a}$) is simulated result in CTRL (ALL)) are shown in Fig.3b&4b, statistically significant at 95% confidence level.~~

~~A negative value of PRD indicates that the bias is smaller compared to CTRL, and vice versa.~~

~~In boreal winter, t~~The global mean SST bias is approximately 0.~~30~~32℃, and the average ~~root mean square error (~~RMSE~~)~~ is about ~~0.90~~1.09℃ from day 4 to day 56 in CTRL (Fig. 3a). The simulated SSTs are~~is~~ generally overestimated, and the large biases (>1.0℃) are mainly distributed in the Southern Ocean. In Fig. 3b, t~~T~~he global-averaged ~~regression coefficients of absolute SST biases in CTRL (absolute value of biases in Fig. 3a) with time~~RMSEs of CTRL (black) increase with time in the first month~~are almost positive everywhere (Fig. S3a in the supplementary), indicating the simulations are drifting from the initial state due to no data assimilation, and~~ and then gradually level off. Compared with CTRL, the RMSEs are reduced continuously in VR12-AL-SC-EN and ALL (yellow and red), but not in Z0-M04 and FLUX (purple and blue).~~indicating that the model biases increase with time.~~

~~Figure 3b shows the correlation coefficients between the absolute CTRL biases and the differences of absolute biases between ALL and CTRL, defined as $|\hat{y_a} - y| - |\hat{y_c} - y|$, where y is OISST or ERA5 data, $\hat{y_c}$ ($\hat{y_a}$) is simulated result in CTRL (ALL).~~

~~Figure 3b shows the distribution of correlation coefficients between the absolute biases with positive regression coefficients in CTRL (absolute value of biases in Fig. 3a) and PRDs in ALL (Fig. 3f) from day 4 to day 56. Only coefficients with P value less than 0.05 are shown. The negative (positive) values indicate that the SST bias in CTRL decreases (increases) with time in the fully coupled ALL experiment. Noticeably, the bias reduction mainly occurs in regions where SST is largely overestimated (>1.0℃), particularly in the Southern Ocean.~~

To understand the key process responsible for the bias reduction in ALL, the ~~global distribution of~~ SST ~~averaged PRD~~differences ~~was~~ are compared across all four experiments (Fig.3c-f). Clearly, the difference ~~distribution of PRD~~ in experiment VR12-AL-SC-EN is similar to that in ALL (Fig. 3c&3f). The spatial correlation coefficient between the SST differences with OISST ~~average PRD distributions~~

of the two experiments (Fig. 3c&3f) is 0.9967, significant at 99% confidence level, and the RMSEs of SST are not different significantly (red and yellow lines in Fig. 3b&5a), indicating the Stokes drift-related parameterizations in VR12-AL-SC-EN, mainly contribute to the SST positive bias reduction. This is different with Couvelard et al. (2020), where –SST overestimations and MLD biasesunderestimations are reduced mainly due to the directly modified turbulence kinetic energyTKE scheme. The global mean SST PRD bias in ALL is– 0.02 ℃ with RMSE of 1.03℃ 7.74±2.21%, and in most areas the PRD SST differences compared with CTRL are significant (P≤0.05) (dotted areas in Fig. 3f). Large SST improvements mainly appear in the Southern Ocean, with a regional mean PRD RMSE decreases from 1.27 to 1.04 ℃ reaching 35.89±9.98% south of 45°S (Fig. 3f and red line in Fig. 5a). The reduction of overestimated SSTs in CTRL (red in Fig 3a) is because the Langmuir turbulenceStokes drift-related parameterizations with Stokes-Coriolis force and entrainmentin MOM4 injects turbulent kinetic energy into the ocean, which enhances vertical mixing, and subsequently cools the surface waters (Belcher et al., 2012; Li et al. 2016). The modified roughness and relative velocity in Z0 FANZ0-M04 and FLUX also influence upper ocean mixing (Fig. 3d&e) via changing momentum flux, but and lead to generally warmer SSTsthe total SST changes are not significant (purple and blue lines in Fig. 3b&5a). The effect from Stokes drift-related ocean mixing parameterizations dominates SST changes in ALL.

In boreal summer, the global mean SST bias in CTRL is overestimated approximately 0.29℃, and the averaged RMSE from day 4 to day 56 is about 0.871.19℃. The overestimated SSTs (>1.0℃) mainly occur in the Northern Hemisphere (Fig. 4a). The global-averaged RMSEs are also generally timeseries show continuous lower values in VR12-AL-SC-EN and ALL than incompared with CTRL, except the last week (Fig. 4b). The cooling effects in VR12-AL-SC-EN lead to a global mean PRD bias of -3.85± 1.32%0.06℃, smaller than that in boreal winter, and the large SST improvements mainly occur north of

50°N (Fig. 4c and yellow line in Fig. 5b). The changes of SST in ~~Z0-FAN~~Z0-M04 and FLUX (Fig. 4d~~,~~ &e; purple and blue lines in Fig. 4b&5b) are ~~again~~ relatively small. The global mean ~~PRD~~ bias in ALL is ~~-3.26±1.13%~~0.04℃ with RMSE of 1.14℃ (Fig. 4f). ~~The correlation coefficients between absolute bias in CTRL (Fig. 4a) and PRD in ALL (Fig. 4f) show significant negative values mainly in the Northern Hemisphere (Fig. 4b), indicating improvements of overestimated SST in ALL. While both positive and negative PRDs of SST appear in the Southern Ocean, probably owing to the insufficient model resolution which could not resolve mesoscale activities.~~

As aforementioned, large improvements of overestimated SST mainly occur at~~in~~ mid~~-and-~~high latitudes in local summer. The time series of RMSEs and correlation coefficients of SST between model and observation in the region (0-360°E, 45°-78°S in boreal winter and 0-360°E, 50°-78°N in boreal summer) are shown in Fig. 5c-f. The RMSE~~s~~ in CTRL (blue in Fig. 5c&d) increase~~s~~ in the first few weeks and then gradually decrease~~s~~ afterward. Compared with CTRL, RMSEs in VR12-AL-SC-EN (yellow) and ALL (red) are significantly ($P \leqslant 0.01$) reduced by about 0.3℃. The spatial correlation coefficients decrease with time but remain high (>0.90) for all experiments (Fig. 5e&f) with higher values in ~~. The~~ experiment~~s ALL and~~ VR12-AL-SC-EN (~~red and~~ yellow)~~. show higher correlation coefficients than CTRL (blue) in boreal summer (Fig. 5f), although the changes are weak in boreal winter (Fig. 5e), indicating that the Stokes drift related ocean mixing plays a dominant role in SST warm bias reduction in high latitudes in summer.~~

We also compared T02 from experiments with ERA5 (Fig. 6). Warm biases of T02 appear in both winter and summer in CTRL (Fig. 6a&b). The changes of ~~distribution of PRD of~~ T02 ~~difference~~ in sensitivity experiments (Fig. 6c-j) ~~is~~ are generally consistent with the changes~~that~~ of SST in the same experiments (Fig.3&4). T~~,~~he correlation coefficients between the SST and the T02 changes for the ALL

experiment in boreal winter and summer (Fig. 3f&6f and Fig. 4f&6j) are 0.61 and 0.53 respectively, significant at 99% confidence level~~, because indicating the surface air temperature is mainly regulated by SST~~. In boreal winter, all wave-coupled experiments except FLUX reduce the T02 mean bias ~~in general~~ (Fig.6c-f). VR12-AL-SC-EC has the largest T02 bias reduction compared with CTRL.~~ The global averaged PRD of bias which decreases~~ from 0.55℃ to 0.~~08~~17~~17~~℃~~is 7.51±0.11%, and the RMSE decreases from 2.72℃ to 2.61℃with reduction exceeding 20% in the Southern Ocean~~ (Fig.6c~~g~~e). ~~The regional T02 RMSE decreases from 1.93 to 1.67 ℃south of 45°S in ALL.~~ In boreal summer, both VR12-AL-SC-EC and ~~bias RMSE of T02 is~~ALL ~~has~~have the largest T02 bias reduction, from 0.29℃ to 0.08℃ (Fig.6g&j). Noticeably, the improvements in RMSEs —are not large for all experiments, because~~slightly increased in the Southern Ocean in all experiments except ALL (Fig.6g-j), although the positive bias is reduced, mainly consistent with the slight SST bias increase in the Southern Ocean (Fig. 4c-f)due to the decrease of T02 overestimation in CTRL~~the improvements mainly occur~~s~~ in areas with overestimated temperature.

4.2 Mixed Layer Depth (MLD)

To further evaluate the direct effect of the wave-related processes on upper ocean, we compared the MLD of all experiments with that estimated from Argo profiles in summer. The simulated T/S were interpolated onto the positions of Argo profiles at the nearest time. The MLD was estimated as the depth where the change of potential density reaches the value corresponding to a 0.2℃ decrease of potential temperature with unchanged salinity from surface (de Boyer Montégut et al., 2004; Wang and Xu, 2018).

The time series of MLDs from numerical experiments and Argo south of 45°S in boreal winter (north of 45°N in boreal summer) are compared in Fig. 7a (7b). The simulated MLDs are generally within the

STD of Argo MLDs (shading in Fig. 7). In CTRL, the mean bias (CTRL minus Argo) with STD is -13.15±7.82 m (-6.75±5.29 m) in boreal winter (summer). The correlation coefficients of MLDs in CTRL with Argo MLDs is 0.55 (0.68) with P ≤0.01, and the mean RMSEs is 15.30 m (8.55 m) in boreal winter (summer). In ALL, the mean bias (ALL minus Argo) with STD is 9.617.70±8.7810.42 m (5.23±7.223.30±7.78 m) in boreal winter (summer), and. tThe correlation coefficient of MLDs south of 45°S (north of 45°N) enhances to 0.690.63 (0.790.78) in boreal winter (summer).. The RMSE south of 45°S decreases from 15.30 m in CTRL to 13.0212.96 m in ALL. The RMSE north of 45°N decreases from 6.71 m in CTRL to 4.93 5.55 m in ALLALL in the first six weeks but the value increases in the last two weeks due –to overestimation of MLDs. Compared with CTRL (orange in Fig. 7), VR12-AL-SC-EN (yellow) and ALL (dark blue) show significantly improvements (P ≤0.01) on the underestimated MLDs time series, whereas the MLDs difference between CTRL and Z0-FANZ0-M04 (purple)/FLUX (blue) is non-significant. –Furthermore, there is no significant difference between VR12-AL-SC-EN and ALL, indicating the Stokes drift-related ocean mixing dominates the total wave effects on MLD in ALL.

4.3 Wind Speed at 10 m (WSP10) and Significant Wave Height (SWH)

Compared with ERA5 In general, the WSP10s in CTRL are generally overestimated in both winter and summer compared with ERA5 (Fig.8a and Fig. &9a). The global averaged RMSEs of WSP10s in CTRL are 3.514.25 m/s (3.534.26 m/s) in boreal winter (summer). The global averaged WSP10 RMSE timeseries The correlation coefficients between absolute bias in CTRL and PRD in ALL are calculated shown where regression coefficients of absolute bias with time are positive in CTRL in (Fig. S3c8b&9b. The global averaged RMSEs of WSP10s in CTRL (black) all experiments increase with time in the first

two weeks and then gradually level off with ~~oscillations~~perturbations (Fig. 8b ~~and Fig. &~~9b)~~d)~~. ~~Only values, significant at 95% confidence level, are shown. The widely distributed negative values indicate decreasing trends of bias in these areas (Fig. 8b&9b).~~ The differences of RMSEs ~~timeseries~~ between CTRL and other experiments are ~~relatively modest~~tiny in the first 10 days, and afterwards~~although~~ the RMSEs in~~those of~~ –Z0-M04 and ALL (purple and red) ~~are~~become clear~~general~~ly ~~lower~~ smaller than in CTRL over most of the time. ~~In addition, the comparisons of WSP10 from numerical experiments with ERA5 (Fig. 8a&9a) indicate that the overestimated (underestimated) SWH (Fig. 10a&11a)~~WSP10 ~~are directly related~~corresponds ~~to~~ to the ~~overestimated (underestimated) WSP10, with the correlation coefficients of 0.59 and 0.55 (Fig. 8a&10a and Fig. 9a&11a) in boreal winter and summer, significant at 99% confidence level~~SWH (Fig. 10a&11a).

The comparisons of the simulated SWHs in CTRL with the ERA5 ~~data over 53 days for boreal winter and boreal summer are shown in Figure 10 and 11, respectively~~ also show that. ~~In boreal winter,~~ the SWHs are overestimated in both winter and summer (Fig. 10a ~~and Fig. &~~11a). In boreal winter, t~~T~~the global mean SWH bias in CTRL is approximately 0.20 m~~, mainly due to the~~ with overestimates (> 0.30 m) in the Pacific, the North Atlantic and the Southern Ocean (Fig.10a), and the average RMSE is about 1.~~04~~ 29 m. In boreal summer, the global mean bias in CTRL is approximately 0.17 m with ~~0.96~~1.22 m RMSE (Fig. 11a). Similar to ~~Fig. 8b&9b~~ WSP10s, ~~in Fig. 10b&11b~~ the ~~SWH~~ RMSEs of SWHs ~~in CTRL (black)~~ also increase in the first two weeks and then gradually level off with ~~oscillations~~perturbations (Fig. 10b ~~and Fig.&~~ 11b)~~The significant negative correlation (Fig. 10b&11b) between absolute bias in CTRL and PRD in ALL appears in most overestimated regions.~~ ~~And t~~The ~~SWH~~ RMSEs in Z0-M04 and ALL (purple and red) are ~~reduced~~smaller than ~~compared with~~ in CTRL ~~for~~over most of the time, consistent with changes of WSP10s~~, especially in boreal winter (Fig. 10b), indicating the improvement~~

~~of overestimated SWH in the fully coupled ALL experiment.~~ The correlation coefficients between changes of WSP10s ~~difference~~ and changes of SWHs ~~difference~~ in ALL are 0.77 and 0.73 in boreal winter and summer respectively (Fig. 8f&10f and Fig. 9f&11f), significant at 99% confidence level, indicating that the SWHs changes are closely related to ~~is originated from the~~changes of –wind speeds ~~change~~.

~~WSP10 and SWH differences between sensitivity experiments and CTRL (sensitivity experiments minus CTRL) are shown (Figs. 8-11 e-f). For boreal winter, i~~In VR12-AL-SC-EN, the reduction of SST warm biases affects air temperature and stabilizes marine atmospheric boundary layer (Sweet et al. 1981; O'Neill et al. 2003), and subsequently reduces WSP10s and SWHs with decreased global ~~averaged~~ bias ~~reduction of 0.31±0.14 m/s and 0.19±0.09 m (Fig.8e&10e), respectively~~ in boreal winter (Fig.8c&10c). In ~~Z0-FAN~~Z0-M04 ~~experiment~~, the overestimated WSP10s and SWHs are also reduced (Fig. 8d&10d) ~~with bias of 0.07 m/s and 0.08 m, and the global averaged bias~~ RMSE ~~reduction is 0.30±0.14 is reduced to 4.15 m/s and 1.14 0.23±0.12 m (Fig. 8d&10d). The changes in WSP10 and SWH stem from~~due to the larger~~updated~~ z_0~~, generated by WW3~~ with the ~~ST4-FAN~~ST4-M04 scheme~~, which is larger than the original z_0 in GFS~~ at wind speed > 10 m/s (Fig. 2). The increase of z_0 enhances wind stress and momentum transferred into the ocean, and therefore reduces surface winds (Pineau-Guillou et al. 2018; Sauvage et al. 2020)~~. Whereas the reduced surface winds decrease z_0 (Fig. 2), therefore in the end the wind stresses are weaker in most areas in Z0-FAN than in CTRL. Since the 10-m wind in GFS is diagnosed from the friction velocity by the well-known logarithmic profile (Charnock, 1955), its change is consistent with wind stress,~~ and consequently reduces SWHs. In FLUX (Fig. 8e&10e), ~~the change of WSP10 and SWH is marginal in terms of global average (Fig. 8e&10e).~~ $\overrightarrow{U_{surf}}$ and $\overrightarrow{u_s(0)}$ ~~in FLUX~~ decrease wind stress and momentum transfer when their directions are consistent with ~~that of~~ wind directions, and vice versa (Hersbach and Bidlot, 2008; Renault et al., 2016). For instance, the angles between wind and current are relatively small (<90°) in the northeastern Pacific, reducing the wind stress and thus enhancing WSP10s (Fig. 8e). In contrast, ~~for these areas~~ the large angles (>90°) between the northwesterlies and the Kuroshio in the northwestern Pacific– ~~can~~enhance wind stress, and decrease WSP10s (Fig. 8e). Consequently, the improvements occur in areas with misalignment of winds and currents. ~~Although the decreased momentum flux into water could increase surface wind (Renault et al., 2016), the effect is rather small in the coupled system with a relative coarse resolution. The effects of $\overrightarrow{U_{surf}}$ and $\overrightarrow{u_s(0)}$ are discussed separately in Section 4.4.~~ With all combined effects, the biases of

WSP10s and SWHs in ALL in most regions ~~tend to~~are decreased (Fig. 8f&10f). ~~compared with CTRL (Fig. 8a&10a), especially for overestimated WSP10 and SWH,~~ with the reduced global RMSEs of 4.17 m/s and 1.18 m respectively.

In boreal summer, the ~~changes~~ improvements of WSP10s and SWHs are relatively small in terms of global averaged ~~average~~RMSEs, because of smaller positive biases in CTRL (Fig. 9a&11a). In ALL, the global averaged bias ~~reduction~~ of WSP10s (SWHs) is ~~reduced to~~ ~~0.14±0.13~~0.01 m/s (~~0.16±0.07~~0.03 m). The largest reduction primarily appears in the Southern Ocean (Fig. 9f&11f) to improve the overestimated westerlies~~y~~ and SWHs in CTRL (Fig. 9a&11a). ~~Notably, the WSP10 and the SWH significantly increase in the south of Australia and the northwestern Pacific in FLUX (Fig. 9e&11e), where they are underestimated in CTRL. The WSP10 and the SWH are enhanced by the modified momentum transfer caused by the Stokes drift and ocean surface current (Fig. S1d&f). Even though, the increases partly vanish in ALL (Fig. 9f&11f) owing to stabilization of atmosphere caused by Stokes drift-related ocean mixing (Fig. 9e&11e) and enhanced roughness (Fig. 9d&11d).~~

Previous studies indicated that ocean surface winds in ERA5 are underestimated in some regions (Belmonte Rivas and Stoffelen 2019; Kalverla et al. 2020; Sharmar and Markina 2020). To better demonstrate the effects of waves on WSP10s and SWHs, ~~we also compared the simulation results with NDBC buoy data (locations shown in Fig. 12, numbers of available buoys marked in Table 2 and buoy identifiers listed in Table S4). the~~ comparisons of WSP10s and SWHs with the NDBC buoy data~~s~~ are made (Table 2 and Fig. 12). ~~shown~~ The differences between sensitivity experiments and CTRL are all statistically significant at 95% confidence level. Buoys ~~in Fig. 12 (locations~~ are mainly located in the northeastern Pacific, the tropical Pacific and the northwestern Atlantic oceans~~shown in~~ (Fig. S3), and buoy identifiers with total numbers, longitudes and latitudes are listed in Table S3~~)~~. The method from Hsu et al. (1994) was used to adjust wind speeds from buoy data to the reference height of 10 m. ~~The x-~~

~~axis is WSP10/SWH of buoys, and the y axis is the ssimulated WSP10/SWH in Jan Feb, 2017 (Fig. 12a&b) and Aug Sep, 2018 (Fig. 12c&d) for all experiments. The bias is reflected by the distance to the y=x line (dotted). The mean biases with standard deviations and RMSEs for every experiment are shown in Table 2. The differences between 4 sensitivity experiments and CTRL are all statistically significant at 95% confidence level.~~

~~In CTRL, C~~ceompared ~~with~~to the NDBC data, the WSP10s and the ~~/~~SWHs in CTRL are~~is~~ generally overestimated in both winter and summer with positive mean biases (Table 2 and Fig. 12). The reduction of mean biases appears in ~~Except the FLUX experiment in Jan-Feb, 2017, a~~all ~~other~~ experiments except FLUX in boreal winter.~~lead to a decrease of mean bias. Therefore,~~ T~~t~~he wave-related processes are most effective in areas with positive biases ~~(above y=x line)~~, consistent with previous comparisons with ERA5.~~ .~~ ~~The contrast~~In boreal winter, ~~–~~the angles between ~~in~~winds and currents are small. The wind stresses ~~is~~are then reduced in ~~–~~FLUX~~-~~, and the WSP10s ~~is~~are enhanced. So the positive bias is further enhanced. ~~for winter (enhanced WSP10s in Fig. 12a) and summer (reduced WSP10s in Fig. 12c) is consistent with the regional angle changes between wind and current analyzed above by generally reducing WSP10 and SWH, which can also be observed in Fig. 12. In ALL experiment,~~The improvements in ALL are generally the largest (Table 2), with the WSP10s RMSE~~s~~ ~~of WSP10~~ of 1.04 m/s (1.15 m/s) and the SWHs RMSE~~s~~ of ~~SWH~~ 0.36 m (0.24 m) in boreal winter (summer).~~–~~ ~~the RMSEs of WSP10 (SWH) decrease from both 1.24 m/s to 1.04 m/s and 1.15 m/s (0.44 m and 0.38 m to 0.36 m and 0.24 m) in Jan Feb, 2017 and Aug Sep, 2018.~~As shown in Fig. 12, with the increase of WSP10s and SWHs, the reduction of overestimation in ALL compared with CTRL ~~the overestimation~~ is more prominent~~heavier in CTRL, and the reduction of overestimation is more obvious. Compared with Jan-Feb, 2017 (Fig. 12a), in Aug Sep, 2018 the improvement of WSP10 simulation is smaller (Fig. 12a&c;~~

RMSEs in Table 2), because of weaker winds in summer than winter.According to the CTRL bias distribution, the biases (CTRL minus NDBC) were sorted into three categories (Table 2), that is, the upper quartile (UQ; the buoys with the highest 25% bias; yellow marks in Fig. 12), the lower quartile (LQ; the buoys with the lowest 25% bias; light blue marks) and the median (MD; the rest 50%; black marks). And the corresponding mean biases in CTRL were given in brackets of Table 2. In general, the UQ/LQ buoys (yellow/light blue in Fig.12) collocate with positive/negative bias between CTRL and ERA5 (shading in Fig. 12), and the MD buoys collocate with mild bias. From Table 2, the biases of both WSP10 and SWH between CTRL and buoy data are positive in both seasons, except for LQ buoys.

The mean biases with standard deviations and RMSEs for every experiment are shown in Table 2. The differences between 4 sensitivity experiments and CTRL are all statistically significant at 95% confidence level.The 53-day mean absolute percentage errors (MAPE=$(\frac{100\%}{n})\sum_{i=1}^{n}\left|\frac{\widehat{y_i}-y_i}{y_i}\right|$, where $\widehat{y_i}$ is simulated value, y_i is NDBC buoy observation, i=1, 53) were calculated. The method from Hsu et al. (1994) was used to adjust wind speeds from buoy data to the reference height of 10 m. The corresponding MAPE differences compared with CTRL for the other four simulations are shown in Table 2, where a negative (positive) value means that the bias is reduced (enhanced) versus CTRL.

In boreal winter, all four experiments lead to significant improvements on WSP10 and SWH for UQ at 95% confidence level. The maximum MAPE difference for WSP10 is -17.31% in FLUX, and -11.93% for SWH in Z0_FAN. While the MAPE differences for LQ are not significant, and the differences for MD are small too. On average, the FLUX experiment shows the best improvement on both WSP10 and SWH, which is -4.97% and -4.43% respectively.

In boreal summer, the MAPE improvements are larger than in boreal winter, and the differences are lower than -10% for WSP10 for UQ in all experiments. This is consistent with the distribution of bias

improvement compared with ERA5 (Figs. 8-11). The largest MAPE difference is -23.21% for WSP10 in FLUX, and -20.05% for SWH in Z0_FAN. Again, the MAPE differences for LQ and MD are relatively small. On average, the largest improvements are shown in FLUX and Z0_FAN, with the MAPE difference of -7.51% and -6.99% for WSP10 and SWH, respectively. Therefore, the wave related processes are most effective in areas with large positive biases. The most effective process varies, depending on seasons and locations.

4.4 Enthalpy Fluxes and Effects of Stokes Drift on Air-Sea Fluxes

The enthalpy fluxes in CTRL are shown in Fig. S4 of supplementary, which are positive upwards. The latent heat flux differences between sensitivity experiments (Table 1) and CTRL are shown in Fig. 13. Note that the distribution of the differences is consistent with those of WSP10 (Fig. 8&9) in general, because the increase of $\Delta\vec{V}$ leads to enhanced upward latent heat flux, and vice versa. Meanwhile, the differences in sensible heat flux between sensitivity experiments and CTRL have similar distribution patterns but weaker magnitude (Fig. S5 of supplementary).

To better understand the effects of current and Stokes drift on air-sea fluxes in CFSv2, two extra experiments with only surface current (FLUX_CURR) or Stokes drift (FLUX_ST) considered in Eqn. 10 were carried out. We compared the difference of momentum flux, latent heat flux and sensible heat flux between FLUX_CURR and CTRL (Fig. S6 in supplementary), as well as FLUX_ST and CTRL (Fig. S7 in supplementary), respectively. Since the effects of $\overrightarrow{U_{surf}}$ and $\overrightarrow{u_s(0)}$ on $\Delta\vec{V}$ depend on their directions, enhanced (reduced) momentum flux and WSP10 occur in areas with relatively large (small) angles with wind (Fig. S1g-j). The angles between Stokes drift and wind are much smaller than those between current and wind, and the large angles in mid-high latitudes and coastal areas are resulted from

~~the dominance of swells. For instance, the northeasterlies over Kuroshio in boreal summer (Fig. S1b) is in alignment with the Stokes drift (Fig. S1f), reducing the wind stress and the WSP10 (Fig. S7b, d). In contrast, the Kuroshio is northeastward (Fig. S1d), enhancing wind stress and WSP10 (Fig. S6b, d).~~

~~Compared with the NDBC data (Fig. 12), the combined effects of the current and the Stokes drift lead to larger MAPE improvements in FLUX than those in both FLUX_CURR and FLUX_ST for WSP10 (Table S3). Note that these effects are stronger in mid and high latitudes in winter due to large winds and large waves. In addition, the latent heat flux as well as the sensible heat flux change consistently with momentum flux (Fig. S6e-h&S7e-h).~~

5 Summary and Discussion

To investigate the individual role played by wave-related processes on atmosphere and ocean interface in a coupled global atmosphere-ocean-wave modeling system on intraseasonal scale, we implemented the version 5.16 of WW3 into CFSv2.0 for global oceans from 78°S-78°N, using the C-Coupler2. In this coupled system, the WW3 was forced by 10-m wind and surface current generated in CG~~G~~FSv2.0. Stokes drift-related Langmuir mixing, Stokes-Coriolis force and entrainment in ocean, air-sea fluxes modified by surface current and Stokes drift, and momentum roughness length (z_0) were considered separately, and the results of sensitivity experiments were compared against in-situ buoys, satellite measurements and ERA5 reanalysis. The effects of waves on intraseasonal prediction were examined in two 56-day cases, one for boreal winter and the other one for boreal summer.

The following key results were found:

1. Overestimated SST, T02 and underestimated MLD in ~~mid-and-high~~mid-high latitudes in CFSv2.0 are significantly improved, particularly in local summer. Because enhanced vertical

mixing generated by Langmuir turbulence, Stokes-Coriolis force and entrainment in VR12-AL-SC-EN changes temperature structure in the upper ocean, and further affects air temperature. In boreal winter~~, for the Southern Ocean~~, ~~the global averaged SST (T02) is improved by 6.90±2.26% (7.51±0.11%). Especially for the Southern Ocean,~~ the ~~the regional mean improvement of SST reaches up to~~ regional RMSE of SST (T02) in the Southern Ocean ~~RMSE~~ decreases from 1.27 (1.93) in CTRL experiment to 1.04 (1.67) ℃ in ALL experiment~~35.89±9.98%~~. In boreal summer, the effect is weaker because of the smaller ocean areas in ~~mid and high~~mid-high latitudes of the Northern Hemisphere~~, with a 3.85±1.32% global mean improvement in SST~~.

2. In general, all wave-related processes lead to reduction of biases for WSP10s and SWHs, particularly in regions where WSP10s and SWHs are overestimated. The decreased SSTs in VR12-AL-SC-EN stabilize~~s~~ marine atmospheric boundary layer, and lead~~s~~ to weakened WSP10s and SWHs. The modified roughness in ~~Z0 FAN~~Z0-M04 generally reduces momentum transfer into the ocean, and so decreases WSP10s and SWHs. The relative wind-wave-current speed in FLUX also affects wind stress, and further influences WSP10s and SWHs. Compared with NDBC buoy observations and ERA5, the ALL experiment shows significant improvements ~~in ALL experiment, the RMSEs of WSP10 decrease from 1.24 m/s (1.24 m/s) to 1.04 m/s (1.15 m/s) and the RMSEs of SWH decrease from 0.44 m (0.38 m) to 0.36 m (0.24 m) in boreal winter (summer)~~or ~~buoys with overestimations in CTRL, in boreal winter the maximum improvement for WSP10 is 17.31% in FLUX, and 11.93% for SWH in Z0 FAN. In boreal summer, the largest improvement is 23.21% for WSP10 in FLUX, and 20.05% for SWH in Z0 FAN~~.

In addition to the variables aforementioned, the changes of simulated enthalpy fluxes were also compared, whichchanges generallymainly depend on the WSP10s changes. However, the wave-related effects on enthalpy fluxes are non-significant for the 2-month simulation, so the results are not shown.

The wave-related parameterizations used in the study mainly improve model biases at mid-high latitudes, andAs shown in Fig. 3&4, SST biases also appear in tropical oceans are only slightly improved (Fig. 3& Fig. 4). , so more wave-related processes might need to be considered in the futureBreivik et al. (2015) improved SST as well as subsurface temperature simulations in Nucleus for European Modelling of the Ocean (NEMO) with parametrizations including the wave-related Charnock parameter, modification of water-side stress with wind input and wave dissipation, wave dissipation-related turbulent kinetic energy flux and the Stokes-Coriolis force. Based on a global NEMO-WW3 coupled framework, Couvelard et al. (2020) modified the Charnock parameter, the Stokes drift-related forces and the Langmuir cell with misalignment of winds and waves, the oceanic surface momentum flux and the turbulence kinetic energy to reduce SST and mixed layer depth (MLD) biases. In addition, sea sprays can enhance air-sea heat fluxes in the tropics (Andreas et al. 2008; Andreas et al. 2015??). We will consider more processes in the future study.modification of ocean-side stress with wind input and wave dissipation, wave dissipation-related turbulent kinetic energy flux, and nonbreaking wave-related mixing. (Breivik et al., 2015; Law-Chune and Aouf, 2018; Bao et al. 2019; Couvelard et al. 2020). In Breivik et al. (2015), considered the surface waves effects including wave-related Charnock parameter, modification of ocean-side stress, wave dissipation-related turbulent kinetic energy flux, Stokes-Coriolis force and Langmuir mixing, the bias of SST simulation in the tropics is reducedIn the work of Breivik et al. (2015), considered the surface waves, the bias of SST simulation in the tropics is reduced mainly due to drag from swells. The similar effect was also shown in the one-way coupled Nucleus for European

~~Modelling of the Ocean (NEMO) model with the Météo France wave model (MFWAM), where the momentum as well as the energy flux across the air-sea interface are refined (Law-Chune and Aouf, 2018). Besides, more wave-related processes should be considered, such as sea spray, wave breaking and non-breaking wave effects (Bao et al. 2019; Couvelard et al. 2020). All these processes are worth future evaluation. In Couvelard et al. (2020) based on the coupling of NEMO and WW3, in addition to Couvelard et al. (2020) the modification of Charnock parameter, the Stokes drift related forces and the Langmuir cell, they furtherly considered the wave-supported stress and the modified turbulence kinetic energy. Besides, the misalignment of wind and waves for Langmuir cells was considered, which leads to weaker mixing than assuming alignment especially in the Southern Ocean. These also generated reasonable improvements of SST and MLD simulation, although the SSTs of control run are generally underestimated but not overestimated in Couvelard et al. (2020). In our system, even the application of VR12-AL (assuming alignment of wind and waves) cannot produce strong enough mixing in the Southern Ocean, and subsequently cannot significantly reduce the warm bias of SST and the shallow bias of MLD. Therefore, we further include the effects of Stokes-Coriolis force and entrainment (VR12-AL-SC-EN) to enhance mixing. While these processes are worth future evaluation.~~

Different parameterizations for the same wave-related process also deserve discussion. For ocean surface roughness, the most classic parametrizations are those developed by Janssen (1989, 1991), Taylor and Yelland (2001) and Drennan et al. (2003). The method of Taylor and Yelland (2001) requires the peak wavelength for the total spectrum, whereas that of Drennan et al. (2003) only requires the peak of wind-sea waves. This difference leads to the fact that the former is more suitable for a mixed sea state, while the latter is more suitable for a young sea state (Drennan et al., 2005). And the effect of Janssen's parameterization (1989, 1991) is similar to that of Drennan et al. (2003), since it is also based on the

wind-sea conditions (Shimura et al., 2017). ~~In addition, Janssen's formulation can be modified to account for the decreased drag coefficient for strong winds (Bidlot et al. 2020; ECMWF 2020), and the parameterization can improve simulation of tropical cyclone (Li et al. 2021).~~

The case studies indicate that there remain significant biases in the coupled system, probably owing to inaccuracy of coarse resolution, absence of a coupled wave-ice modular, and deficiency of initial fields. In addition, to further improve the model and eliminate the biases, as Breivik et al. (2015) proposed, extra adjusting of the individual model components in the coupled systems is also necessary. All of these require further efforts to investigate efficient methods to improve fully coupled systems.

Code and data availability

The code developed for the coupled system can be found under https://doi.org/10.5281/zenodo.5811002~~10.5281/zenodo.5109521~~ (Shi et al., ~~2020~~2021), including the coupling, preprocessing, run control and postprocessing scripts. The initial fields for CFSv2.0 are generated by the real time operational Climate Data Assimilation System, downloaded from the CFSv2.0 official website (http://nomads.ncep.noaa.gov/pub/data/nccf/com/cfs/prod). The daily average satellite Optimum Interpolation SST (OISST) data are obtained from NOAA (https://www.ncdc.noaa.gov/oisst), and the National Data Buoy Center (NDBC) buoy data are also obtained from NOAA (https://www.ndbc.noaa.gov). The Argo observational profiles of T/S are available at China Argo Real-time Data Center (www.argo.org.cn). The ERA5 reanalysis are available at the Copernicus Climate Change Service (C3S) Climate Date Store (https://cds.climate.copernicus.eu/cdsapp#!/dataset/reanalysis-era5-single-levels).

Author contribution

FX and RS designed the experiments and RS carried them out. RS developed the code of coupling parametrizations and produced the figures. ZF contributed to the installation and operation of CFSv2.0. LL and HY contributed to the application of C-Coupler2. XL and YZ provided the original code of CFSv2.0. RS prepared the manuscript with contributions from all co-authors. FX and HL contributed to review and editing.

Acknowledgments

The authors would like to extend thanks to all developers of the CFSv2.0 model (https://cfs.ncep.noaa.gov/cfsv2/downloads.html). The work was supported by National Key Research and Development Program of China (no. 2016YFC1401408), and Tsinghua University Initiative Scientific Research Program (2019Z07L01001). We also thank two anonymous reviewers for their constructive comments.

References

Andreas, E. L., Mahrt, L., and Vickers, D.: An improved bulk air-sea surface flux algorithm, including spray-mediated transfer, Quarterly Journal of the Royal Meteorological Society, 141, 642-654, 2015.

Andreas, E. L., Persson, P. O. G., and Hare, J. E.: A bulk turbulent air–sea flux algorithm for high-wind, spray conditions, Journal of Physical Oceanography, 38, 1581-1596, 2008.

Ardhuin, F., Rogers, E., Babanin, A. V., Filipot, J., Magne, R., Roland, A., Der Westhuysen, A. V., Queffeulou, P., Lefevre, J. M., and Aouf, L.: Semiempirical Dissipation Source Functions for Ocean Waves. Part I: Definition, Calibration, and Validation, Journal of Physical Oceanography, 40, 1917-1941, http://dx.doi.org/10.1175/2010JPO4324.1, 2010.

Atlas, R., Hoffman, R. N., Ardizzone, J., Leidner, S. M., Jusem, J. C., Smith, D. K., and Gombos, D.: A Cross-calibrated, Multiplatform Ocean Surface Wind Velocity Product for Meteorological and Oceanographic Applications, Bulletin of the American Meteorological Society, 92, 157-174, http://dx.doi.org/10.1175/2010BAMS2946.1, 2011.

Bao, Y., Song, Z., & Qiao, F.: FIO-ESM version 2.0: Model description and evaluation. Journal of Geophysical Research: Oceans, 125, e2019JC016036. https://doi.org/10.1029/2019JC016036, 2019.

Belcher, S. E., Grant, A. L. M., Hanley, K., Foxkemper, B., Van Roekel, L., Sullivan, P. P., Large, W. G., Brown, A. R., Hines, A., and Calvert, D.: A global perspective on Langmuir turbulence in the ocean surface boundary layer, Geophysical Research Letters, 39, http://dx.doi.org/10.1029/2012GL052932, 2012.

Beljaars, A. C. M.: The parametrization of surface fluxes in large-scale models under free convection. Q. J. R. Meteorol. Soc., 121, 255{270. https://doi.org/10.1002/qj.49712152203, 1994.

Belmonte Rivas, M., and Stoffelen, A.: Characterizing ERA-Interim and ERA5 surface wind biases using ASCAT, Ocean Science, 15, 831-852, 10.5194/os-15-831-2019, 2019.

Bidlot, J.-R., Prates, F., Ribas, R., et al.: Enhancing tropical cyclone wind forecasts, ECMWF newsletter, 164, 33-37. https://www.ecmwf.int/en/newsletter/164/meteorology/enhancing-tropical-cyclonewind-forecasts, 2020.

Bidlot, J.-R.: Model upgrade improves ocean wave forecasts. ECMWF newsletter, 159, 10-10. https://www.ecmwf.int/en/newsletter/159/news/modelupgrade-improves-ocean-wave-forecasts, 2019.

Bidlot, J.-R.: Present status of wave forecasting at ECMWF, Workshop on ocean waves, 25-27, 2012.

Breivik, Ø., Bidlot, J.-R., and Janssen, P. A.: A Stokes drift approximation based on the Phillips spectrum, Ocean Modelling, 100, 49-56, 2016.

Breivik, Ø., Janssen, P. A., and Bidlot, J.-R.: Approximate Stokes drift profiles in deep water, Journal of Physical Oceanography, 44, 2433-2445, 2014.

Breivik, Ø., Mogensen, K., Bidlot, J., Balmaseda, M., and Janssen, P. A. E. M.: Surface wave effects in the NEMO ocean model: Forced and coupled experiments, Journal of Geophysical Research, 120, 2973-2992, http://dx.doi.org/10.1002/2014JC010565, 2015.

Charnock, H.: Wind stress on a water surface, Quarterly Journal of the Royal Meteorological Society, 81, 639-640, http://dx.doi.org/10.1002/qj.49708135027, 1955.

Couvelard, X., Lemarié, F., Samson, G., Redelsperger, J.-L., Ardhuin, F., Benshila, R., and Madec, G.: Development of a two-way-coupled ocean-wave model: assessment on a global NEMO(v3.6)-WW3(v6.02) coupled configuration, Geosci. Model Dev., 13, 3067-3090, https://doi.org/10.5194/gmd-13-3067-2020, 2020.

de Boyer Montégut, C., Madec, G., Fischer, A. S., Lazar, A., and Iudicone, D.: Mixed layer depth over the global ocean: An examination of profile data and a profile - based climatology, Journal of Geophysical Research, 109, http://dx.doi.org/10.1029/2004JC002378, 2004.

Donelan, M. A., Haus, B. K., Reul, N., Plant, W. J., Stiassnie, M., Graber, H. C., Brown, O. B., and Saltzman, E. S.: On the limiting aerodynamic roughness of the ocean in very strong winds, Geophysical Research Letters, 31, 10.1029/2004gl019460, 2004.

Drennan, W. M., H. C. Graber, D. Hauser, and C. Quentin: On the wave age dependence of wind stress over pure wind seas, J. Geophys. Res., 108(C3), 8062, doi:10.1029/2000JC000715, 2003.

Drennan, W. M., P. K. Taylor, and M. J. Yelland: Parameterizing the sea surface roughness, J. Phys. Oceanogr., 35(5), 835-848, 2005.

826 ECMWF: Official IFS Documentation CY47R1. In chap. PART VII: ECMWF wave model. Reading,
827 UK: ECMWF, 10.21957/31drbygag, 2020.
828 Fan, Y., Lin, S., Held, I. M., Yu, Z., and Tolman, H. L.: Global Ocean Surface Wave Simulation Using a
829 Coupled Atmosphere–Wave Model, Journal of Climate, 25, 6233-6252, http://dx.doi.org/10.1175/JCLI-
830 D-11-00621.1, 2012.
831 Ghantous, M., and Babanin, A. V.: One-dimensional modelling of upper ocean mixing by turbulence due
832 to wave orbital motion, Nonlinear Processes in Geophysics, 21, 325-338, 10.5194/npg-21-325-2014,
833 2014.
834 Griffies, S. M., Harrison, M. J., Pacanowski, R. C., and Rosati, A.: A technical guide to MOM4, GFDL
835 Ocean Group Tech. Rep, 5, 342, 2004.
836 Hasselmann, K.: Wave-driven inertial oscillations, Geophysical and Astrophysical Fluid Dynamics, 1,
837 463-502, http://dx.doi.org/10.1080/03091927009365783, 1970.
838 Hersbach H. and Bidlot, J.-R.: The relevance of ocean surface current in the ECMWF analysis and
839 forecast system. Proceeding from the ECMWF Workshop on Atmosphere-Ocean Interaction, 10-12,
840 https://www.ecmwf.int/sites/default/files/elibrary/2009/9866-relevance-ocean-surface-current-ecmwf-
841 analysis-and-forecast-system.pdf, 2008.
842 Hersbach, H., Bell, B., Berrisford, P., Hirahara, S., et al.: The ERA5 Global Reanalysis, Quarterly Journal
843 of the Royal Meteorological Society, Soc. 00: 363 (2020), https://doi.org/10.1002/qj.3803, 2020.
844 Hsu, S. A., Eric A. Meindl, and David B. Gilhousen: Determining the Power-Law Wind-Profile Exponent
845 under Near-Neutral Stability Conditions at Sea, Applied Meteorology, Vol. 33, No. 6,
846 https://doi.org/10.1175/1520-0450(1994)033<0757:DTPLWP>2.0.CO;2, 1994.

Janssen, P. A. E. M.: The interaction of ocean waves and wind, Cambridge University Press, pp 312, 2004.

Janssen, P. A. E. M.: The Quasi-linear theory of wind wave generation applied to wave forecasting. J. Phys. Oceanogr. 21, 1631-1642. https://doi.org/10.1175/1520-0485(1991)021<1631:QLTOWW>2.0.CO;2, 1991.

Janssen, P. A. E. M.: Wave-induced stress and the drag of air flow over sea waves. J. Phys. Oceanogr. 19(6), 745-754. https://doi.org/10.1175/1520-1310 0485(1989)019<0745:WISATD>2.0.CO;2, 1989.

Kalnay, E., Kanamitsu, M., Kistler, R., Collins, W. D., Deaven, D. G., Gandin, L. S., Iredell, M. D., Saha, S., White, G. H., and Woollen, J.: The NCEP/NCAR 40-Year Reanalysis Project, Bulletin of the American Meteorological Society, 77, 437-471, http://dx.doi.org/10.1175/1520-0477(1996)077%3C0437:TNYRP%3E2.0.CO;2, 1996.

Kalverla, P. C., Holtslag, A. A. M., Ronda, R. J., and Steeneveld, G.-J.: Quality of wind characteristics in recent wind atlases over the North Sea, Quarterly Journal of the Royal Meteorological Society, 146, 1498-1515, 10.1002/qj.3748, 2020.

Kukulka, T., Plueddemann, A. J., Trowbridge, J. H., and Sullivan, P. P.: Significance of Langmuir circulation in upper ocean mixing: comparison of observations and simulations, Geophysical Research Letters, 36, http://dx.doi.org/10.1029/2009GL037620, 2009.

Law-Chune, S., and Aouf, L.: Wave effects in global ocean modeling: parametrizations vs. forcing from a wave model, Ocean Dynamics, 68, 1739-1758, http://dx.doi.org/10.1007/s10236-018-1220-2, 2018.

Lemarié, F.: Numerical modification of atmospheric models to include the feedback of oceanic currents on air-sea fluxes in ocean-atmosphere coupled models, INRIA Grenoble-Rhône-Alpes, Laboratoire Jean Kuntzmann, https://hal.inria.fr/hal-01184711/document, 2015.

Li, D., Staneva, J., Bidlot, J.-R., Grayek, S., Zhu, Y., and Yin, B.: Improving Regional Model Skills During Typhoon Events: A Case Study for Super Typhoon Lingling Over the Northwest Pacific Ocean, Frontiers in Marine Science, 8, 10.3389/fmars.2021.613913, 2021.

Li, M., and Garrett, C.: Mixed Layer Deepening Due to Langmuir Circulation, Journal of Physical Oceanography, 27, 121-132, http://dx.doi.org/10.1175/1520-0485(1997)027%3C0121:MLDDTL%3E2.0.CO;2, 1997.

Li, Q., Foxkemper, B., Breivik, O., and Webb, A.: Statistical models of global Langmuir mixing, Ocean Modelling, 113, 95-114, http://dx.doi.org/10.1016/j.ocemod.2017.03.016, 2017.

Li, Q., Webb, A., Foxkemper, B., Craig, A., Danabasoglu, G., Large, W. G., and Vertenstein, M.: Langmuir mixing effects on global climate: WAVEWATCH III in CESM, Ocean Modelling, 103, 145-160, http://dx.doi.org/10.1016/j.ocemod.2015.07.020, 2016.

Li, Z., Liu, Z., & Xing, X.: User Manual for Global Argo Observational data set (V3.0) (1997-2019), China Argo Real-time Data Center, Hangzhou, 37pp, 2019.

Liu, L., Zhang, C., Li, R., and Wang, B.: C-Coupler2: a flexible and user-friendly community coupler for model coupling and nesting, Geoscientific Model Development Discussions, 11, 1-63, http://dx.doi.org/10.5194/gmd-11-3557-2018, 2018.

Luo, J.J., Masson, S., Roeckner, E., Madec, G., & Yamagata, T.: Reducing climatology Bias in an ocean-atmosphere CGCM with improved coupling physics. Journal of Climate, 18(13), 2344-2360. https://doi.org/10.1175/JCLI3404.1, 2005.

Mcwilliams, J. C., and Sullivan, P. P.: Vertical Mixing by Langmuir Circulations, Spill Science & Technology Bulletin, 6, 225-237, http://dx.doi.org/10.1016/S1353-2561(01)00041-X, 2000.

Moon, I., Ginis, I., and Hara, T.: Effect of surface waves on Charnock coefficient under tropical cyclones, Geophysical Research Letters, 31, http://dx.doi.org/10.1029/2004GL020988, 2004.

Moum J.N., and Smyth W.D.: Upper Ocean Mixing. In Cochran, J. Kirk; Bokuniewicz, J. Henry; Yager, L. Patricia (Eds.) Encyclopedia of Ocean Sciences, 3rd Edition. vol. 1, pp. 71-79, Elsevier. ISBN: 978-0-12-813081-0, 2019.

O'Neill, L. W., Chelton, D. B., and Esbensen, S. K.: Observations of SST-induced perturbations of the wind stress field over the Southern Ocean on seasonal timescales, Journal of Climate, 16, 2340-2354, 10.1175/2780.1, 2003.

Pineau-Guillou L., Ardhuin,F., Bouin,M.N.,Redelsperger,J.L.,Chapron,B., Bidlot, J. R., & Quilfen, Y.: Strong winds in a coupled wave-atmosphere model during a North Atlantic storm event: evaluation against observations. Quarterly Journal of the Royal Meteorological Society, 144(711), 317-332, 2018.

Polonichko, V.: Generation of Langmuir circulation for nonaligned wind stress and the Stokes drift, J. Geophys. Res., 102, 15773– 15780, https://doi.org/10.1029/97JC00460, 1997.

Powell, M. D., Vickery, P. J., and Reinhold, T. A.: Reduced drag coefficient for high wind speeds in tropical cyclones, Nature, 422, 279-283, 10.1038/nature01481, 2003.

Qiao, F., Yuan, Y., Yang, Y., Zheng, Q., Xia, C., and Ma, J.: Wave‐induced mixing in the upper ocean: Distribution and application to a global ocean circulation model, Geophysical Research Letters, 31, http://dx.doi.org/10.1029/2004GL019824, 2004.

Renault, L., Arsouze, T., and Ballabrera-Poy, J.: On the Influence of the Current Feedback to the Atmosphere on the Western Mediterranean Sea Dynamics, Journal of Geophysical Research-Oceans, 126, 10.1029/2020jc016664, 2021.

911 Renault, L., Molemaker, M. J., McWilliams, J. C., Shchepetkin, A. F., Lemarie, F., Chelton, D., Illig, S.,
912 and Hall, A.: Modulation of Wind Work by Oceanic Current Interaction with the Atmosphere, Journal of
913 Physical Oceanography, 46, 1685-1704, 10.1175/jpo-d-15-0232.1, 2016.
914 Reynolds, R. W., Smith, T. M., Liu, C., Chelton, D. B., Casey, K. S., and Schlax, M. G.: Daily High-
915 Resolution-Blended Analyses for Sea Surface Temperature, Journal of Climate, 20, 5473-5496,
916 http://dx.doi.org/10.1175/2007JCLI1824.1, 2007.
917 Saha, S., Moorthi, S., Pan, H., Wu, X., Wang, J., Nadiga, S., Tripp, P., Kistler, R., Woollen, J., and
918 Behringer, D.: The NCEP Climate Forecast System Reanalysis, Bulletin of the American Meteorological
919 Society, 91, 1015-1057, http://dx.doi.org/10.1175/2010BAMS3001.1, 2010.
920 Saha, S., Moorthi, S., Wu, X., Wang, J., Nadiga, S., Tripp, P., Behringer, D., Hou, Y., Chuang, H., and
921 Iredell, M. D.: The NCEP Climate Forecast System Version 2, Journal of Climate, 27, 2185-2208,
922 http://dx.doi.org/10.1175/JCLI-D-12-00823.1, 2014.
923 Sauvage, C., Lebeaupin Brossier, C., Bouin, M. N., & Ducrocq, V.: Characterization of the air-sea
924 exchange mechanisms during a Mediterranean heavy precipitation event using realistic sea state
925 modelling. Atmospheric Chemistry & Physics, 20(3), 2020.
926 Sharmar, V., and Markina, M.: Validation of global wind wave hindcasts using ERA5, MERRA2, ERA-
927 Interim and CFSRv2 reanalyzes, IOP Conference Series: Earth and Environmental Science, 606, 012056
928 (012059 pp.)-012056 (012059 pp.), 10.1088/1755-1315/606/1/012056, 2020.
929 Shimura, T., Mori, N., Takemi, T., et al.: Long term impacts of ocean wave-dependent roughness on
930 global climate systems. Journal of Geophysical Research: Oceans, 122(3),
931 https://doi.org/10.1002/2016JC012621, 2017.

Stopa, J. E., Ardhuin, F., Babanin, A. V., and Zieger, S.: Comparison and validation of physical wave parameterizations in spectral wave models, Ocean Modelling, 103, 2-17, http://dx.doi.org/10.1016/j.ocemod.2015.09.003, 2016.

Sweet, W., Fett, R., Kerling, J., and Laviolette, P.: Air–sea interaction effects in the lower troposphere across the north wall of the Gulf Stream, Mon. Weather Rev., 109, 1042-1052, 10.1175/1520-0493(1981)109<1042:Asieit>2.0.Co;2, 1981.

Takatama, K., and Schneider, N.: The Role of Back Pressure in the Atmospheric Response to Surface Stress Induced by the Kuroshio, Journal of the Atmospheric Sciences, 74, 597-615, 10.1175/jas-d-16-0149.1, 2017.

Taylor, P. K., and Yelland, M. J.: The Dependence of Sea Surface Roughness on the Height and Steepness of the Waves, Journal of Physical Oceanography, 31, 572-590, http://dx.doi.org/10.1175/1520-0485(2001)031%3C0572:TDOSSR%3E2.0.CO;2, 2001.

Terray, E. A., Donelan, M. A., Agrawal, Y. C., Drennan, W. M., Kahma, K. K., Williams, A. J., Hwang, P. A., and Kitaigorodskii, S. A.: Estimates of Kinetic Energy Dissipation under Breaking Waves, Journal of Physical Oceanography, 26, 792-807, http://dx.doi.org/10.1175/1520-0485(1996)026%3C0792:EOKEDU%3E2.0.CO;2, 1996.

Tolman, H. L., and Chalikov, D. V.: Source Terms in a Third-Generation Wind Wave Model, Journal of Physical Oceanography, 26, 2497-2518, http://dx.doi.org/10.1175/1520-0485(1996)026%3C2497:STIATG%3E2.0.CO;2, 1996.

Van Roekel, L. P., Foxkemper, B., Sullivan, P. P., Hamlington, P. E., and Haney, S.: The form and orientation of Langmuir cells for misaligned winds and waves, Journal of Geophysical Research, 117, http://dx.doi.org/10.1029/2011JC007516, 2012.

Wang, L., and Xu, F.: Decadal variability and trends of oceanic barrier layers in tropical Pacific, Ocean Dynamics, 68, 1155-1168, 10.1007/s10236-018-1191-3, 2018.

WAVEWATCH III Development Group.: User manual and system documentation of WAVEWATCH III version 5.16, NOAA/NWS/NCEP/MMAB Technical Note 329, 326, 2016.

Wu, L., Staneva, J., Breivik, Ø., Rutgersson, A., Nurser, A. G., Clementi, E., and Madec, G.: Wave effects on coastal upwelling and water level, Ocean Modelling, 140, 101405, 2019.

Wu, X., K. S. Moorthi, K. Okomoto, and H. L. Pan: Sea ice impacts on GFS forecasts at high latitudes, Proceedings of the 85th AMS Annual Meeting, 8th Conference on Polar Meteorology and Oceanography, San Diego, CA, 2005.

Zieger, S., Babanin, A. V., Rogers, W. E., and Young, I. R.: Observation-based source terms in the third-generation wave model WAVEWATCH, Ocean Modelling, 96, 2-25, http://dx.doi.org/10.1016/j.ocemod.2015.07.014, 2015.~~Ardhuin, F., Rogers, E., Babanin, A. V., Filipot, J., Magne, R., Roland, A., Der Westhuysen, A. V., Queffeulou, P., Lefevre, J. M., and Aouf, L.: Semiempirical Dissipation Source Functions for Ocean Waves. Part I: Definition, Calibration, and Validation, Journal of Physical Oceanography, 40, 1917-1941, http://dx.doi.org/10.1175/2010JPO4324.1, 2010.~~

~~Atlas, R., Hoffman, R. N., Ardizzone, J., Leidner, S. M., Jusem, J. C., Smith, D. K., and Gombos, D.: A Cross-calibrated, Multiplatform Ocean Surface Wind Velocity Product for Meteorological and Oceanographic Applications, Bulletin of the American Meteorological Society, 92, 157-174, http://dx.doi.org/10.1175/2010BAMS2946.1, 2011.~~

~~Bao, Y., Song, Z., & Qiao, F.: FIO-ESM version 2.0: Model description and evaluation. Journal of Geophysical Research: Oceans, 125, e2019JC016036. https://doi.org/10.1029/2019JC016036, 2019.~~

Belcher, S. E., Grant, A. L. M., Hanley, K., Foxkemper, B., Van Roekel, L., Sullivan, P. P., Large, W. G., Brown, A. R., Hines, A., and Calvert, D.: A global perspective on Langmuir turbulence in the ocean surface boundary layer, Geophysical Research Letters, 39, http://dx.doi.org/10.1029/2012GL052932, 2012.

Beljaars, A. C. M.: The parametrization of surface fluxes in large-scale models under free convection. Q. J. R. Meteorol. Soc., 121, 255{270. https://doi.org/10.1002/qj.49712152203, 1994.

Belmonte Rivas, M., and Stoffelen, A.: Characterizing ERA-Interim and ERA5 surface wind biases using ASCAT, Ocean Science, 15, 831-852, 10.5194/os-15-831-2019, 2019.

Bidlot, J., Prates, F., Ribas, R., et al.: Enhancing tropical cyclone wind forecasts, ECMWF newsletter, 164, 33-37. https://www.ecmwf.int/en/newsletter/164/meteorology/enhancing-tropical-cyclonewind-forecasts, 2020.

Bidlot, J.: Model upgrade improves ocean wave forecasts. ECMWF newsletter, 159, 10-10. https://www.ecmwf.int/en/newsletter/159/news/modelupgrade-improves-ocean-wave-forecasts, 2019.

Bidlot, J. R.: Present status of wave forecasting at ECMWF, Workshop on ocean waves, 2012, 25-27.

Breivik, O., Mogensen, K., Bidlot, J., Balmaseda, M., and Janssen, P. A. E. M.: Surface wave effects in the NEMO ocean model: Forced and coupled experiments, Journal of Geophysical Research, 120, 2973-2992, http://dx.doi.org/10.1002/2014JC010565, 2015.

Charnock, H.: Wind stress on a water surface, Quarterly Journal of the Royal Meteorological Society, 81, 639-640, http://dx.doi.org/10.1002/qj.49708135027, 1955.

Couvelard, X., Lemarié, F., Samson, G., Redelsperger, J. L., Ardhuin, F., Benshila, R., and Madec, G.: Development of a two-way-coupled ocean-wave model: assessment on a global NEMO(v3.6)-

997 WW3(v6.02) coupled configuration, Geosci. Model Dev., 13, 3067–3090, https://doi.org/10.5194/gmd-
998 13-3067-2020, 2020.
999 de Boyer Montégut, C., Madec, G., Fischer, A. S., Lazar, A., and Iudicone, D.: Mixed layer depth over
1000 the global ocean: An examination of profile data and a profile - based climatology, Journal of
1001 Geophysical Research, 109, http://dx.doi.org/10.1029/2004JC002378, 2004.
1002 Donelan, M. A., Haus, B. K., Reul, N., Plant, W. J., Stiassnie, M., Graber, H. C., Brown, O. B., and
1003 Saltzman, E. S.: On the limiting aerodynamic roughness of the ocean in very strong winds, Geophysical
1004 Research Letters, 31, 10.1029/2004gl019460, 2004.
1005 Drennan, W. M., H. C. Graber, D. Hauser, and C. Quentin: On the wave age dependence of wind stress
1006 over pure wind seas, J. Geophys. Res., 108(C3), 8062, doi:10.1029/2000JC000715, 2003.
1007 Drennan, W. M., P. K. Taylor, and M. J. Yelland: Parameterizing the sea surface roughness, J. Phys.
1008 Oceanogr., 35(5), 835–848, 2005.
1009 ECMWF: Official IFS Documentation CY47R1. In chap. PART VII: ECMWF wave model. Reading,
1010 UK: ECMWF, 10.21957/31drbygag, 2020.
1011 Fan, Y., and Griffies, S. M.: Impacts of Parameterized Langmuir Turbulence and Nonbreaking Wave
1012 Mixing in Global Climate Simulations, Journal of Climate, 27, 4752–4775,
1013 http://dx.doi.org/10.1175/JCLI-D-13-00583.1, 2014.
1014 Fan, Y., Lin, S., Held, I. M., Yu, Z., and Tolman, H. L.: Global Ocean Surface Wave Simulation Using a
1015 Coupled Atmosphere–Wave Model, Journal of Climate, 25, 6233–6252, http://dx.doi.org/10.1175/JCLI-
1016 D-11-00621.1, 2012.

Fox-Kemper, B., Adcroft, A., Boning, C. W., Chassignet, E. P., Curchitser, E. N., Danabasoglu, G., Eden, C., England, M. H., Gerdes, R., and Greatbatch, R. J.: Challenges and Prospects in Ocean Circulation Models, Frontiers in Marine Science, 6, 65, http://dx.doi.org/10.3389/fmars.2019.00065, 2019.

Ghantous, M., and Babanin, A. V.: One-dimensional modelling of upper ocean mixing by turbulence due to wave orbital motion, Nonlinear Processes in Geophysics, 21, 325-338, 10.5194/npg-21-325-2014, 2014.

Griffies, S. M., Harrison, M. J., Pacanowski, R. C., and Rosati, A.: A technical guide to MOM4, GFDL Ocean Group Tech. Rep, 5, 342, 2004.

Hasselmann, K.: Wave-driven inertial oscillations, Geophysical and Astrophysical Fluid Dynamics, 1, 463-502, http://dx.doi.org/10.1080/03091927009365783, 1970.

Hersbach H. and Bidlot, J. R.: The relevance of ocean surface current in the ECMWF analysis and forecast system. Proceeding from the ECMWF Workshop on Atmosphere-Ocean Interaction, 10-12, https://www.ecmwf.int/sites/default/files/elibrary/2009/9866-relevance-ocean-surface-current-ecmwf-analysis-and-forecast-system.pdf, 2008.

Hersbach, H., Bell, B., Berrisford, P., Hirahara, S., et al.: The ERA5 Global Reanalysis, Quarterly Journal of the Royal Meteorological Society, Soc. 00: 363 (2020), https://doi.org/10.1002/qj.3803, 2020.

Hsu, S. A., Eric A. Meindl, and David B. Gilhousen: Determining the Power-Law Wind-Profile Exponent under Near-Neutral Stability Conditions at Sea, Applied Meteorology, Vol. 33, No. 6, https://doi.org/10.1175/1520-0450(1994)033<0757:DTPLWP>2.0.CO;2, 1994.

Janssen, P. A. E. M., and Bidlot, J. R.: Progress in Operational Wave Forecasting, in: Iutam Symposium on Wind Waves, edited by: Grimshaw, R., Hunt, J., and Johnson, E., Procedia IUTAM, 14-29, 2018.

Janssen, P. A. E. M.: The interaction of ocean waves and wind, Cambridge University Press, pp 312, 2004.

Janssen, P. A. E. M.: The Quasi linear theory of wind wave generation applied to wave forecasting. J. Phys. Oceanogr. 21, 1631 1642. https://doi.org/10.1175/1520-0485(1991)021<1631:QLTOWW>2.0.CO;2, 1991.

Janssen, P. A. E. M.: Wave induced stress and the drag of air flow over sea waves. J. Phys. Oceanogr. 19(6), 745 754. https://doi.org/10.1175/1520 1310 0485(1989)019<0745:WISATD>2.0.CO;2, 1989.

Kalnay, E., Kanamitsu, M., Kistler, R., Collins, W. D., Deaven, D. G., Gandin, L. S., Iredell, M. D., Saha, S., White, G. H., and Woollen, J.: The NCEP/NCAR 40 Year Reanalysis Project, Bulletin of the American Meteorological Society, 77, 437-471, http://dx.doi.org/10.1175/1520-0477(1996)077%3C0437:TNYRP%3E2.0.CO;2, 1996.

Kalverla, P. C., Holtslag, A. A. M., Ronda, R. J., and Steeneveld, G. J.: Quality of wind characteristics in recent wind atlases over the North Sea, Quarterly Journal of the Royal Meteorological Society, 146, 1498 1515, 10.1002/qj.3748, 2020.

Kukulka, T., Plueddemann, A. J., Trowbridge, J. H., and Sullivan, P. P.: Significance of Langmuir circulation in upper ocean mixing: comparison of observations and simulations, Geophysical Research Letters, 36, http://dx.doi.org/10.1029/2009GL037620, 2009.

Law Chune, S., and Aouf, L.: Wave effects in global ocean modeling: parametrizations vs. forcing from a wave model, Ocean Dynamics, 68, 1739 1758, http://dx.doi.org/10.1007/s10236 018 1220 2, 2018.

Li, D., Staneva, J., Bidlot, J. R., Grayek, S., Zhu, Y., and Yin, B.: Improving Regional Model Skills During Typhoon Events: A Case Study for Super Typhoon Lingling Over the Northwest Pacific Ocean, Frontiers in Marine Science, 8, 10.3389/fmars.2021.613913, 2021.

Li, M., and Garrett, C.: Mixed Layer Deepening Due to Langmuir Circulation, Journal of Physical Oceanography, 27, 121-132, http://dx.doi.org/10.1175/1520-0485(1997)027%3C0121:MLDDTL%3E2.0.CO;2, 1997.

Li, Q., Foxkemper, B., Breivik, O., and Webb, A.: Statistical models of global Langmuir mixing, Ocean Modelling, 113, 95-114, http://dx.doi.org/10.1016/j.ocemod.2017.03.016, 2017.

Li, Q., Webb, A., Foxkemper, B., Craig, A., Danabasoglu, G., Large, W. G., and Vertenstein, M.: Langmuir mixing effects on global climate: WAVEWATCH III in CESM, Ocean Modelling, 103, 145-160, http://dx.doi.org/10.1016/j.ocemod.2015.07.020, 2016.

Li, Z., Liu, Z., & Xing, X.: User Manual for Global Argo Observational data set (V3.0) (1997-2019), China Argo Real-time Data Center, Hangzhou, 37pp, 2019.

Liu, L., Zhang, C., Li, R., and Wang, B.: C-Coupler2: a flexible and user-friendly community coupler for model coupling and nesting, Geoscientific Model Development Discussions, 11, 1-63, http://dx.doi.org/10.5194/gmd-11-3557-2018, 2018.

Luo, J.J., Masson, S., Roeckner, E., Madec, G., & Yamagata, T.: Reducing climatology Bias in an ocean-atmosphere CGCM with improved coupling physics. Journal of Climate, 18(13), 2344-2360. https://doi.org/10.1175/JCLI3404.1, 2005.

Mcwilliams, J. C., and Sullivan, P. P.: Vertical Mixing by Langmuir Circulations, Spill Science & Technology Bulletin, 6, 225-237, http://dx.doi.org/10.1016/S1353-2561(01)00041-X, 2000.

Moon, I., Ginis, I., and Hara, T.: Effect of surface waves on Charnock coefficient under tropical cyclones, Geophysical Research Letters, 31, http://dx.doi.org/10.1029/2004GL020988, 2004.

Moum J.N., and Smyth W.D.: Upper Ocean Mixing. In Cochran, J. Kirk; Bokuniewicz, J. Henry; Yager, L. Patricia (Eds.) Encyclopedia of Ocean Sciences, 3rd Edition. vol. 1, pp. 71–79, Elsevier. ISBN: 978-0-12-813081-0, 2019.

O'Neill, L. W., Chelton, D. B., and Esbensen, S. K.: Observations of SST-induced perturbations of the wind stress field over the Southern Ocean on seasonal timescales, Journal of Climate, 16, 2340–2354, 10.1175/2780.1, 2003.

Pianezze, J., Barthe, C., Bielli, S., Tulet, P., Jullien, S., Cambon, G., Bousquet, O., Claeys, M., and Cordier, E.: A New Coupled Ocean‐Waves‐Atmosphere Model Designed for Tropical Storm Studies: Example of Tropical Cyclone Bejisa (2013–2014) in the South‐West Indian Ocean, Journal of Advances in Modeling Earth Systems, 10, 801-825, http://dx.doi.org/10.1002/2017MS001177, 2018.

Pineau-Guillou L., Ardhuin,F., Bouin,M.N.,Redelsperger,J.L.,Chapron,B., Bidlot, J. R., & Quilfen, Y.: Strong winds in a coupled wave-atmosphere model during a North Atlantic storm event: evaluation against observations. Quarterly Journal of the Royal Meteorological Society, 144(711), 317-332, 2018.

Powell, M. D., Vickery, P. J., and Reinhold, T. A.: Reduced drag coefficient for high wind speeds in tropical cyclones, Nature, 422, 279-283, 10.1038/nature01481, 2003.

Prakash, K. R., Nigam, T., and Pant, V.: Estimation of oceanic subsurface mixing under a severe cyclonic storm using a coupled atmosphere ocean wave model, Ocean Science, 14, 259-272, http://dx.doi.org/10.5194/os-14-259-2018, 2018.

Qiao, F., Yuan, Y., Ezer, T., Xia, C., Yang, Y., Lu, X., and Song, Z.: A three-dimensional surface wave–ocean circulation coupled model and its initial testing, Ocean Dynamics, 60, 1339-1355, http://dx.doi.org/10.1007/s10236-010-0326-y, 2010.

Qiao, F., Yuan, Y., Yang, Y., Zheng, Q., Xia, C., and Ma, J.: Wave - induced mixing in the upper ocean: Distribution and application to a global ocean circulation model, Geophysical Research Letters, 31, http://dx.doi.org/10.1029/2004GL019824, 2004.

Renault, L., Arsouze, T., and Ballabrera Poy, J.: On the Influence of the Current Feedback to the Atmosphere on the Western Mediterranean Sea Dynamics, Journal of Geophysical Research Oceans, 126, 10.1029/2020jc016664, 2021.

Renault, L., J. Chiggiato, J. C. Warner, M. Gomez, G. Vizoso, and J. TintorèA: Coupled atmosphere-ocean-wave simulations of a storm event over the Gulf of Lion and Balearic Sea, J. Geophys. Res., 117, C09019, doi:10.1029/2012JC007924, 2012.

Renault, L., Molemaker, M. J., McWilliams, J. C., Shchepetkin, A. F., Lemarie, F., Chelton, D., Illig, S., and Hall, A.: Modulation of Wind Work by Oceanic Current Interaction with the Atmosphere, Journal of Physical Oceanography, 46, 1685-1704, 10.1175/jpo-d-15-0232.1, 2016.

Reynolds, R. W., Smith, T. M., Liu, C., Chelton, D. B., Casey, K. S., and Schlax, M. G.: Daily High-Resolution-Blended Analyses for Sea Surface Temperature, Journal of Climate, 20, 5473-5496, http://dx.doi.org/10.1175/2007JCLI1824.1, 2007.

Ricchi, A., Miglietta, M. M., Barbariol, F., Benetazzo, A., Bergamasco, A., Bonaldo, D., Cassardo, C., Falcieri, F. M., Modugno, G., and Russo, A.: Sensitivity of a Mediterranean Tropical-Like Cyclone to Different Model Configurations and Coupling Strategies, Atmosphere, 8, 92, http://dx.doi.org/10.3390/atmos8050092, 2017.

Saha, S., Moorthi, S., Pan, H., Wu, X., Wang, J., Nadiga, S., Tripp, P., Kistler, R., Woollen, J., and Behringer, D.: The NCEP Climate Forecast System Reanalysis, Bulletin of the American Meteorological Society, 91, 1015-1057, http://dx.doi.org/10.1175/2010BAMS3001.1, 2010.

Saha, S., Moorthi, S., Wu, X., Wang, J., Nadiga, S., Tripp, P., Behringer, D., Hou, Y., Chuang, H., and Iredell, M. D.: The NCEP Climate Forecast System Version 2, Journal of Climate, 27, 2185-2208, http://dx.doi.org/10.1175/JCLI-D-12-00823.1, 2014.

Sauvage, C., Lebeaupin Brossier, C., Bouin, M. N., & Ducrocq, V.: Characterization of the air-sea exchange mechanisms during a Mediterranean heavy precipitation event using realistic sea state modelling. Atmospheric Chemistry & Physics, 20(3), 2020.

Sharmar, V., and Markina, M.: Validation of global wind wave hindcasts using ERA5, MERRA2, ERA-Interim and CFSRv2 reanalyzes, IOP Conference Series: Earth and Environmental Science, 606, 012056 (012059 pp.) 012056 (012059 pp.), 10.1088/1755-1315/606/1/012056, 2020.

Shimura, T., Mori, N., Takemi, T., et al.: Long-term impacts of ocean wave-dependent roughness on global climate systems. Journal of Geophysical Research: Oceans, 122(3), https://doi.org/10.1002/2016JC012621, 2017.

Stopa, J. E., Ardhuin, F., Babanin, A. V., and Zieger, S.: Comparison and validation of physical wave parameterizations in spectral wave models, Ocean Modelling, 103, 2-17, http://dx.doi.org/10.1016/j.ocemod.2015.09.003, 2016.

Sun, J., Wei, Z., Xu, T., Sun, M., Liu, K., Yang, Y., Chen, L., Zhao, H., Yin, X., and Feng, W.: Development of a fine-resolution atmosphere-wave-ocean coupled forecasting model for the South China Sea and its adjacent seas, Acta Oceanologica Sinica, 38, 154-166, http://dx.doi.org/10.1007/s13131-019-1419-1, 2019.

Sweet, W., Fett, R., Kerling, J., and Laviolette, P.: Air-sea interaction effects in the lower troposphere across the north wall of the Gulf Stream, Mon. Weather Rev., 109, 1042-1052, 10.1175/1520-0493(1981)109<1042:Asieit>2.0.Co;2, 1981.

Takatama, K., and Schneider, N.: The Role of Back Pressure in the Atmospheric Response to Surface Stress Induced by the Kuroshio, Journal of the Atmospheric Sciences, 74, 597-615, 10.1175/jas-d-16-0149.1, 2017.

Taylor, P. K., and Yelland, M. J.: The Dependence of Sea Surface Roughness on the Height and Steepness of the Waves, Journal of Physical Oceanography, 31, 572-590, http://dx.doi.org/10.1175/1520-0485(2001)031%3C0572:TDOSSR%3E2.0.CO;2, 2001.

Terray, E. A., Donelan, M. A., Agrawal, Y. C., Drennan, W. M., Kahma, K. K., Williams, A. J., Hwang, P. A., and Kitaigorodskii, S. A.: Estimates of Kinetic Energy Dissipation under Breaking Waves, Journal of Physical Oceanography, 26, 792-807, http://dx.doi.org/10.1175/1520-0485(1996)026%3C0792:EOKEDU%3E2.0.CO;2, 1996.

Tolman, H. L., and Chalikov, D. V.: Source Terms in a Third-Generation Wind Wave Model, Journal of Physical Oceanography, 26, 2497-2518, http://dx.doi.org/10.1175/1520-0485(1996)026%3C2497:STIATG%3E2.0.CO;2, 1996.

Van Roekel, L. P., Fox-kemper, B., Sullivan, P. P., Hamlington, P. E., and Haney, S.: The form and orientation of Langmuir cells for misaligned winds and waves, Journal of Geophysical Research, 117, http://dx.doi.org/10.1029/2011JC007516, 2012.

Varlas, G., Vervatis, V., Spyrou, C., Papadopoulou, E., Papadopoulos, A., & Katsafa dos, P.: Investigating the impact of atmosphere-wave-ocean interactions on a Mediterranean tropical-like cyclone. Ocean Modelling, 153, 101675, 2020.

Wang, L., and Xu, F.: Decadal variability and trends of oceanic barrier layers in tropical Pacific, Ocean Dynamics, 68, 1155-1168, 10.1007/s10236-018-1191-3, 2018.

Warner, J. C., Armstrong, B., He, R., and Zambon, J. B.: Development of a Coupled Ocean–Atmosphere–Wave–Sediment Transport (COAWST) Modeling System, Ocean Modelling, 35, 230–244, http://dx.doi.org/10.1016/j.ocemod.2010.07.010, 2010.

WAVEWATCH III Development Group.: User manual and system documentation of WAVEWATCH III version 5.16, NOAA/NWS/NCEP/MMAB Technical Note 329, 326, 2016.

Wu, Z., Jiang, C., Chen, J., Long, Y., Deng, B., and Liu, X.: Three-Dimensional Temperature Field Change in the South China Sea during Typhoon Kai-Tak (1213) Based on a Fully Coupled Atmosphere–Wave–Ocean Model, Water, 11, 140, http://dx.doi.org/10.3390/w11010140, 2019.

Zieger, S., Babanin, A. V., Rogers, W. E., and Young, I. R.: Observation-based source terms in the third-generation wave model WAVEWATCH, Ocean Modelling, 96, 2–25, http://dx.doi.org/10.1016/j.ocemod.2015.07.014, 2015.

Table 1. List of numerical experiments: setups different from CTRL are marked with bold

Experiments	Physical Process/Parameterization		
	Langmuir Cell with Stokes-Coriolis Force and Entrainment	Roughness (Charnock Parameter)	Relative Velocity in Flux
CTRL	Off	Off	Off
VR12-AL-SC-EN	**Eqn. 1-6, 8-10**	Off	Off
Z0-M04	Off	**C_{ch} from Eqn. 16, 17**	Off
FLUX	Off	Off	**$\Delta\vec{V}$ from Eqn. 14**
ALL	**Eqn. 1-6, 8-10**	**C_{ch} from Eqn. 16, 17**	**$\Delta\vec{V}$ from Eqn. 14**

Table 2. The 53-day mean bias with standard deviation (STD) and RMSE for WSP10 and SWH compared with NDBC buoy observation: the bias is calculated as simulation minus NDBC.

Boreal Winter WSP10	**Bias with STD**	**RMSE**
CTRL	0.16±1.23	1.24
VR12-AL-SC-EN	0.01±1.12	1.12
Z0-M04	-0.01±1.07	1.07
FLUX	0.39±1.20	1.26
ALL	0.07±1.04	1.04
Boreal Winter SWH	**Bias with STD**	**RMSE**
CTRL	0.21±0.38	0.44
VR12-AL-SC-EN	0.14±0.35	0.37
Z0-M04	0.10±0.30	0.32
FLUX	0.24±0.34	0.42
ALL	0.12±0.34	0.36
Boreal Summer WSP10	**Bias with STD**	**RMSE**
CTRL	0.15±1.23	1.24
VR12-AL-SC-EN	-0.03±1.22	1.22
Z0-M04	-0.04±1.21	1.21
FLUX	-0.22±1.18	1.20
ALL	-0.17±1.14	1.15
Boreal Summer SWH	**Bias with STD**	**RMSE**
CTRL	0.28±0.25	0.38
VR12-AL-SC-EN	0.19±0.24	0.30
Z0-M04	0.22±0.26	0.34
FLUX	0.14±0.25	0.29
ALL	0.12±0.21	0.24

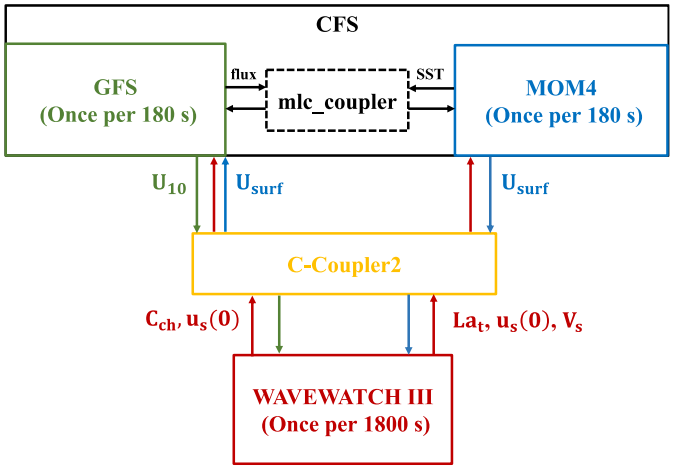

Figure 1. A schematic diagram of the atmosphere-ocean-wave coupled modeling system. The arrows indicate the coupled variables that are passed between the model components. In the diagram, C_{ch}, La_t, $u_s(0)$, V_s, U_{10}, and U_{surf} are Charnock parameter (red arrows), turbulent Langmuir number (red arrows), surface Stokes drift velocity (red arrows), Stokes transport (red arrows), 10-m wind (green arrows) and surface current (blue arrows), respectively.

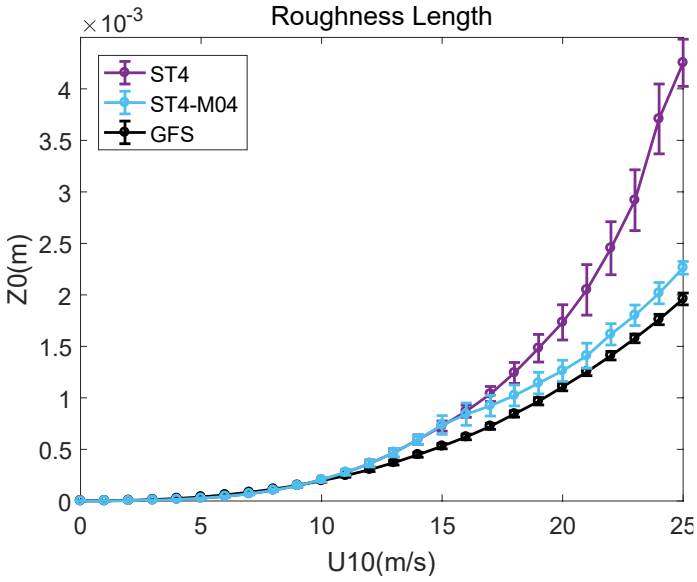

Figure 2. Relationships between momentum roughness length z_0 (m) in the coupled system and 10-m wind speed (m/s); error bars indicate twice the standard deviations for each point.

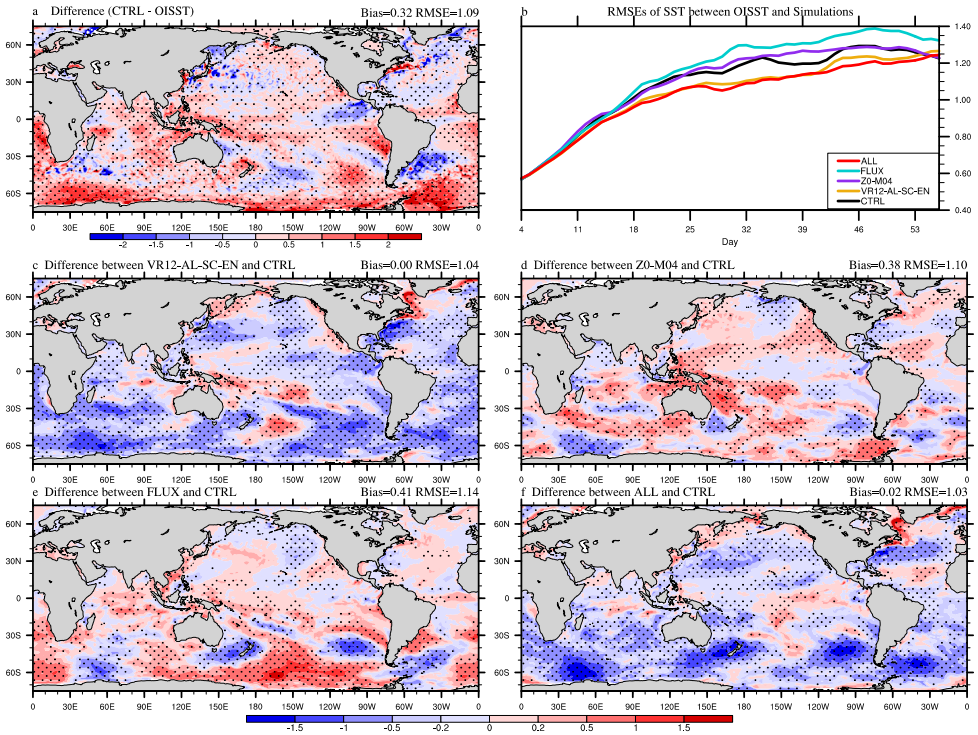

Figure 3. The 53-day average SST (°C) bias in CTRL (a; CTRL minus OISST), the time series of global-averaged RMSE (b), and the differences between VR12-AL-SC-EN (c)/Z0-M04 (d)/ FLUX (e)/ ALL (f) and CTRL in Jan-Feb, 2017 (VR12-AL-SC-EN/Z0-M04/FLUX/ALL minus CTRL). The first 3-day simulation is discarded. The dotted areas are statistically significant at 95% confidence level.

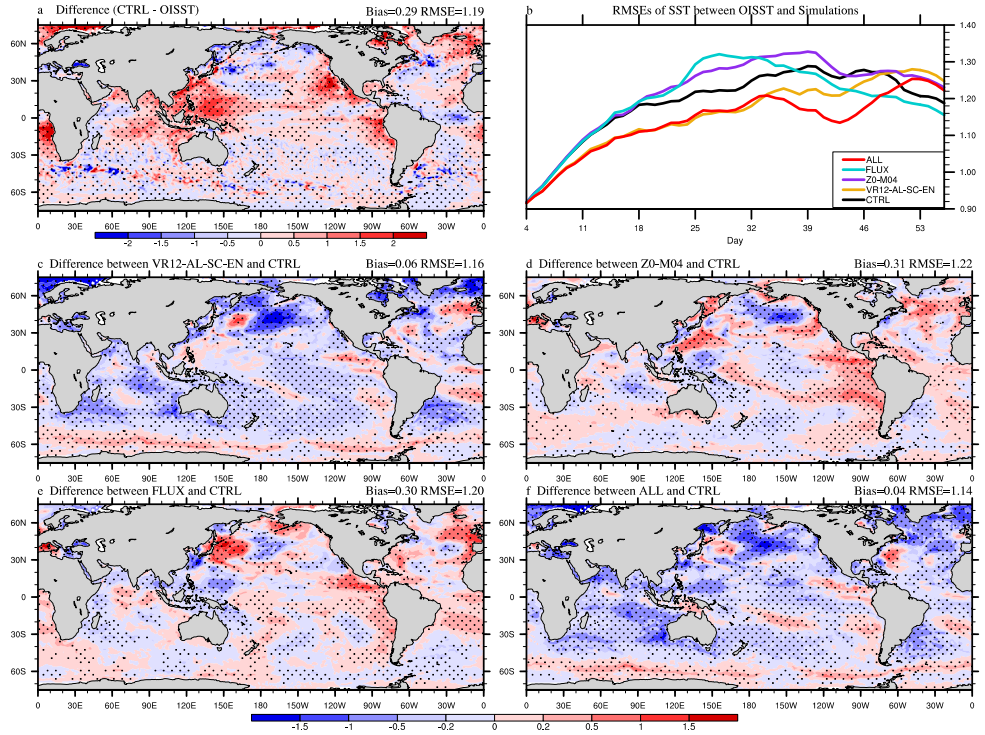

Figure 4. The same as Figure 3 but for Aug-Sep, 2018.

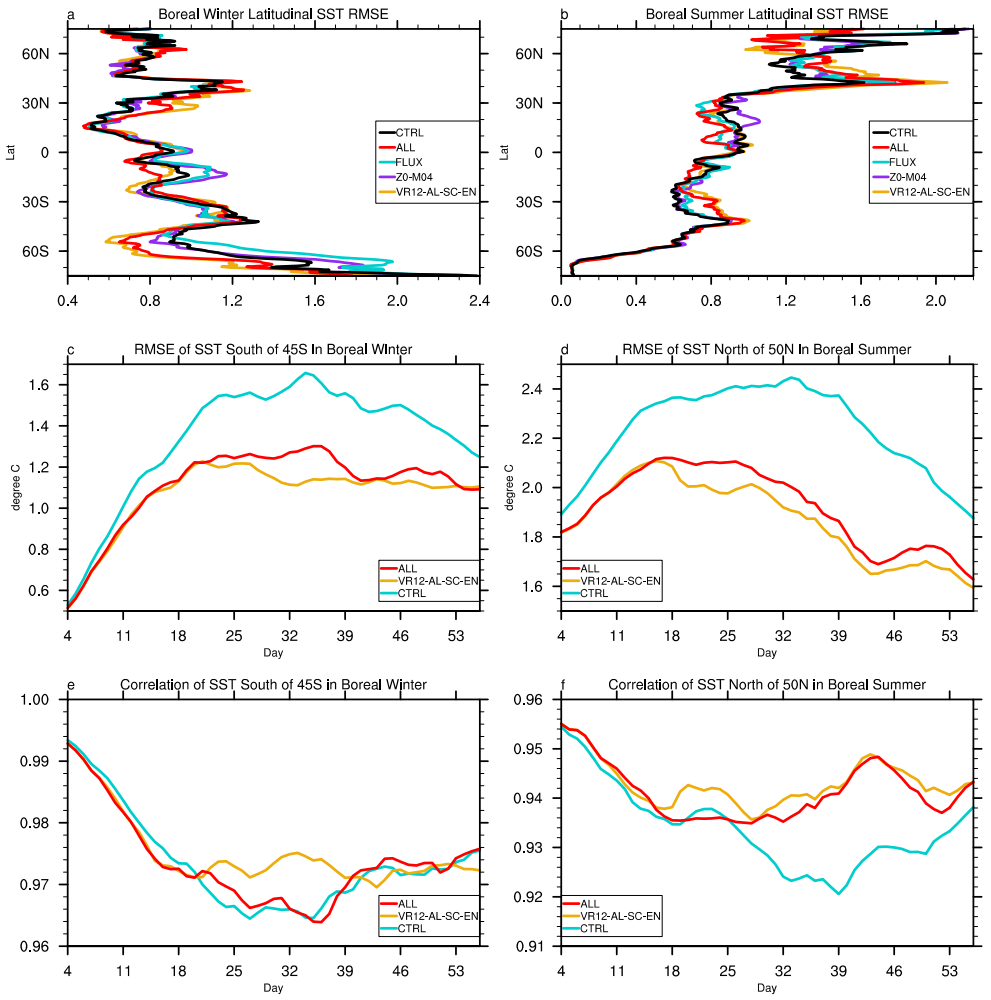

Figure 5. The 53-day averaged latitudinal distribution of SST root mean square errors (RMSE), time series of domain-averaged SST RMSE and correlation coefficient: **a/b** the latitudinal RMSE in boreal winter/summer compared with OISST, **c/d** the time series of domain-averaged (0-360°E, 45-78°S/50-78°N) SST RMSE in boreal winter/summer, **e/f** the time series of domain-averaged (0-360°E, 45-78°S/50-78°N) SST correlation coefficient in boreal winter/summer; differences of RMSE and correlation coefficient time series between VR12-AL-SC-EN/ALL and CTRL are statistically significant at 99% confidence level, except those in Fig. e.

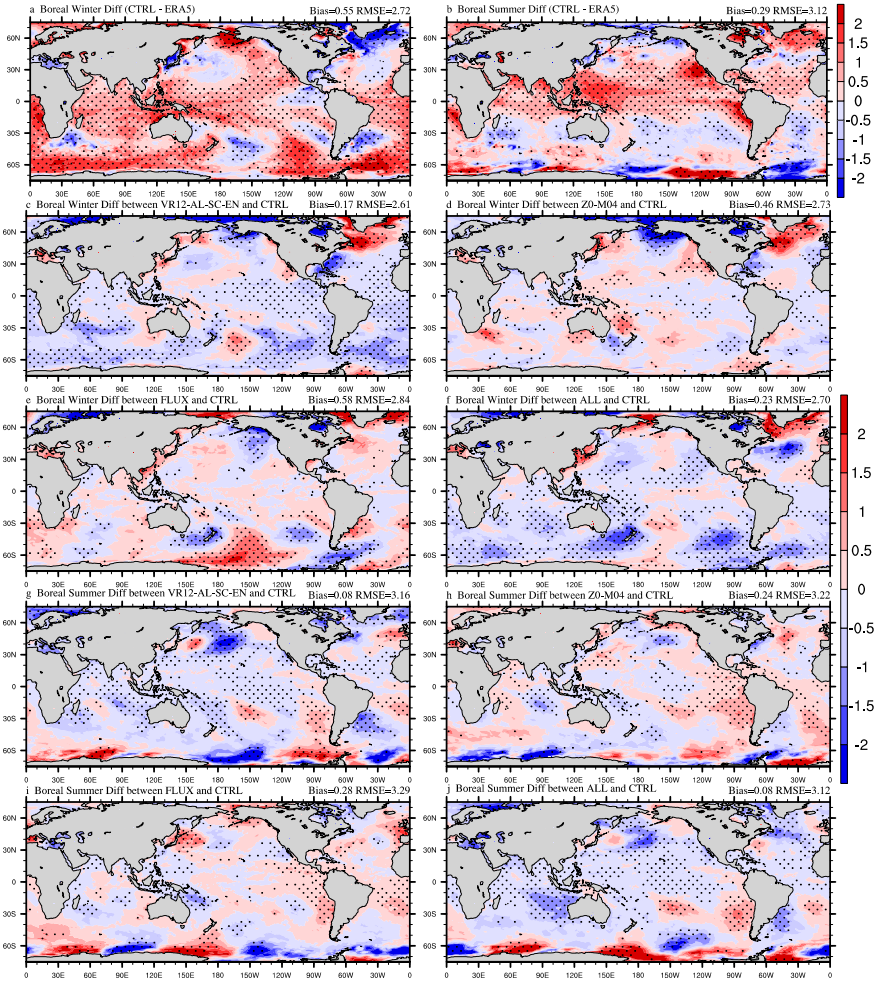

Figure 6. The 53-day average T02 (°C) bias in CTRL (a&b; CTRL minus ERA5), and the differences between VR12-AL-SC-EN (c&g)/Z0-M04 (d&h)/ FLUX (e&i)/ ALL (f&j) and CTRL (VR12-AL-SC-EN/Z0-M04/FLUX/ALL minus CTRL). The first 3-day simulation is discarded. The dotted areas are statistically significant at 95% confidence level. a/c/d/e/f are for Jan-Feb, 2017, and b/g/h/i/j are for Aug-Sep, 2018.

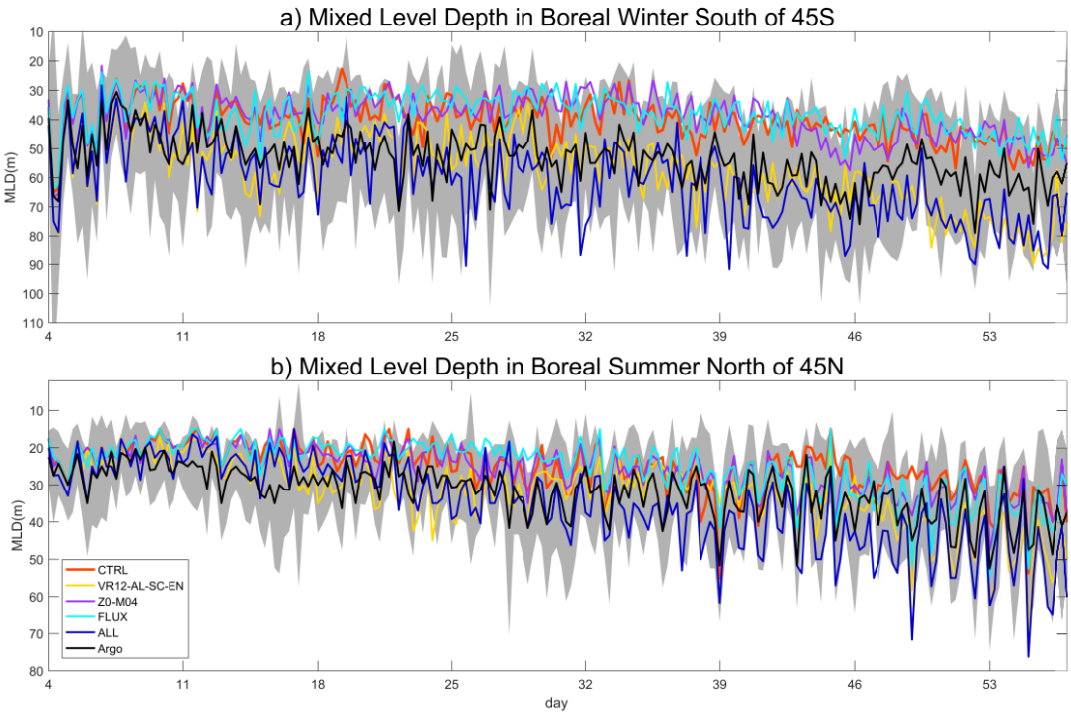

Figure 7. The 53-day time series of domain-averaged (0-360°E, 45-78°S/N) mixed layer depth (MLD; m) in boreal winter/summer: the difference between CTRL and VR12-AL-SC-EN/ALL passes the student's t-test at 99% confidence level; the time intervals are 6 hours; shaded areas indicate twice the standard deviations for Argo.

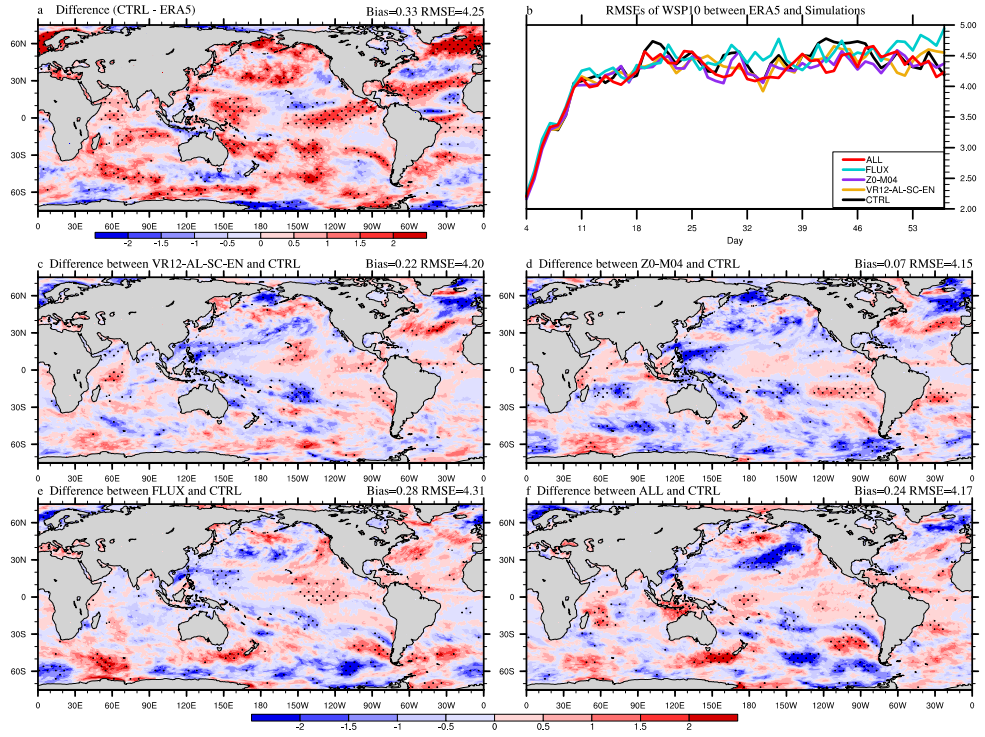

Figure 8. The 53-day average WSP10 (m/s) bias in CTRL (a; CTRL minus ERA5), the time series of global-averaged RMSE (b), and the differences between VR12-AL-SC-EN (c)/Z0-M04 (d)/ FLUX (e)/ ALL (f) and CTRL in Jan-Feb, 2017 (VR12-AL-SC-EN/Z0-M04/FLUX/ALL minus CTRL). The first 3-day simulation is discarded. The dotted areas are statistically significant at 95% confidence level.

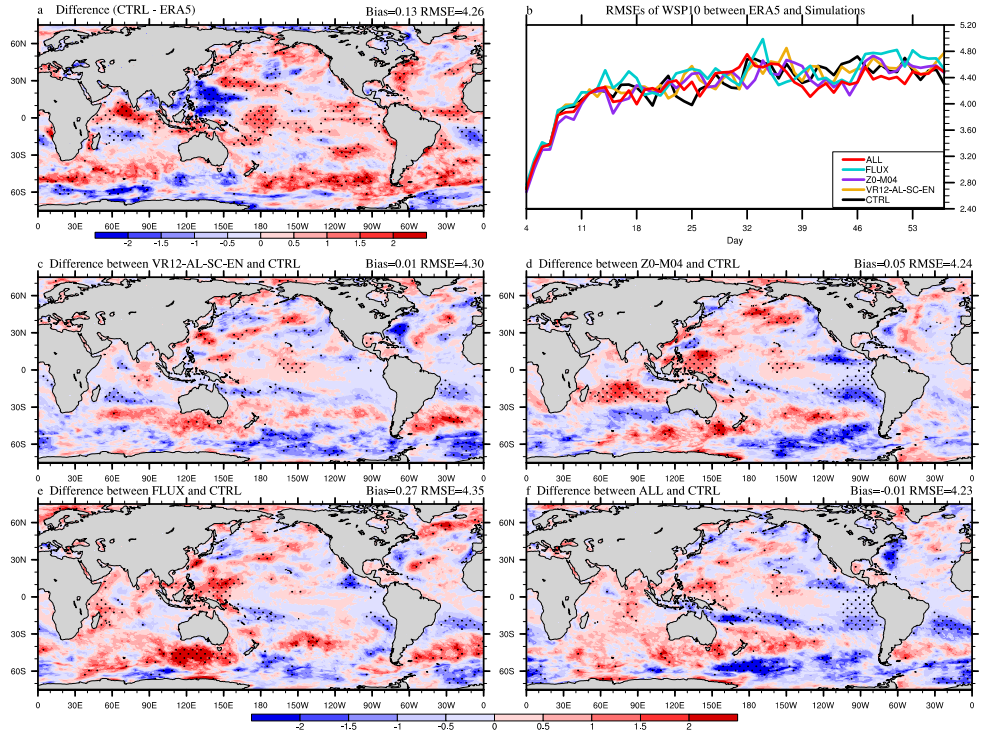

Figure 9. The same as Figure 8 but for Aug-Sep, 2018.

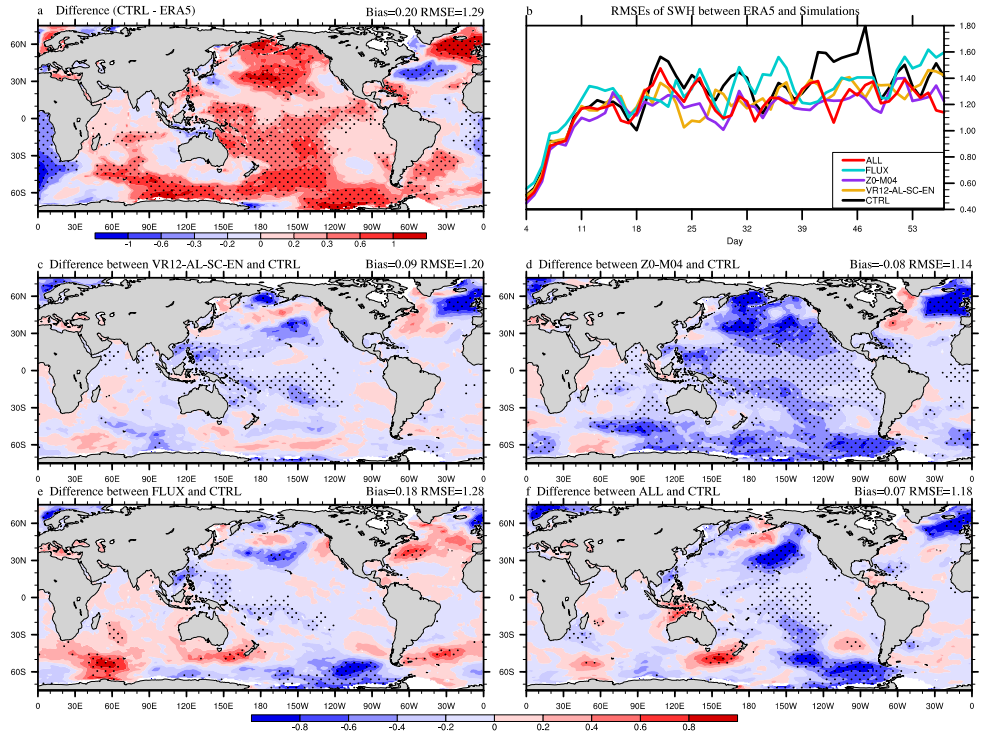

Figure 10. The 53-day average SWH (m) bias in CTRL (a; CTRL minus ERA5), the time series of global-averaged RMSE (b), and the differences between VR12-AL-SC-EN (c)/Z0-M04 (d)/ FLUX (e)/ ALL (f) and CTRL in Jan-Feb, 2017 (VR12-AL-SC-EN/Z0-M04/FLUX/ALL minus CTRL). The first 3-day simulation is discarded. The dotted areas are statistically significant at 95% confidence level.

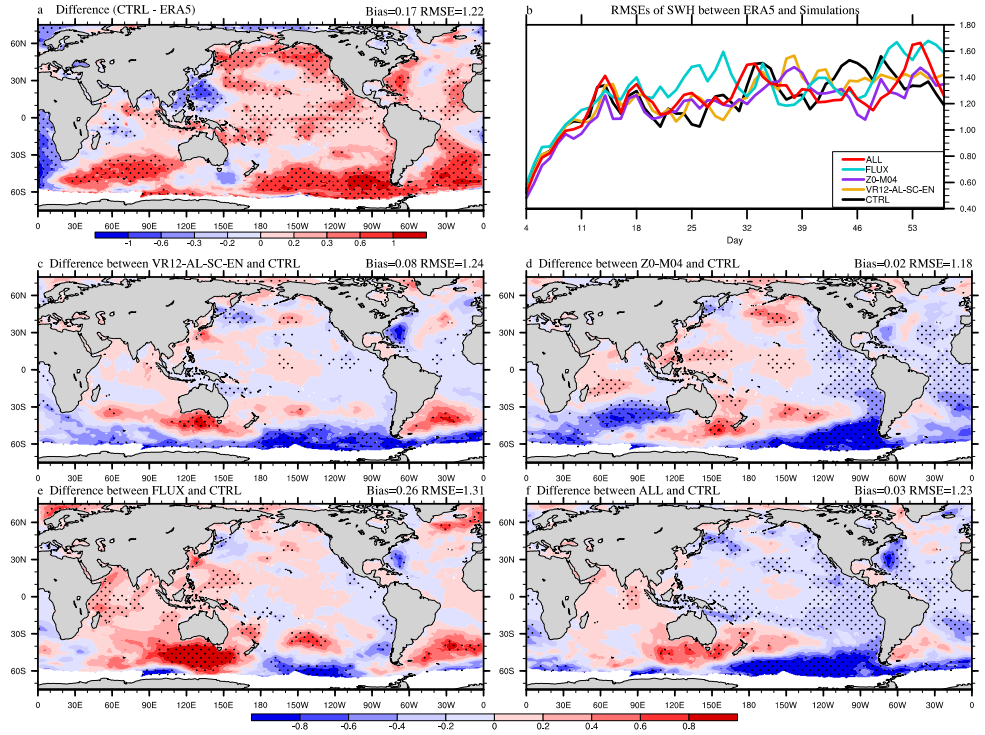

Figure 11. The same as Figure 10 but for Aug-Sep, 2018.

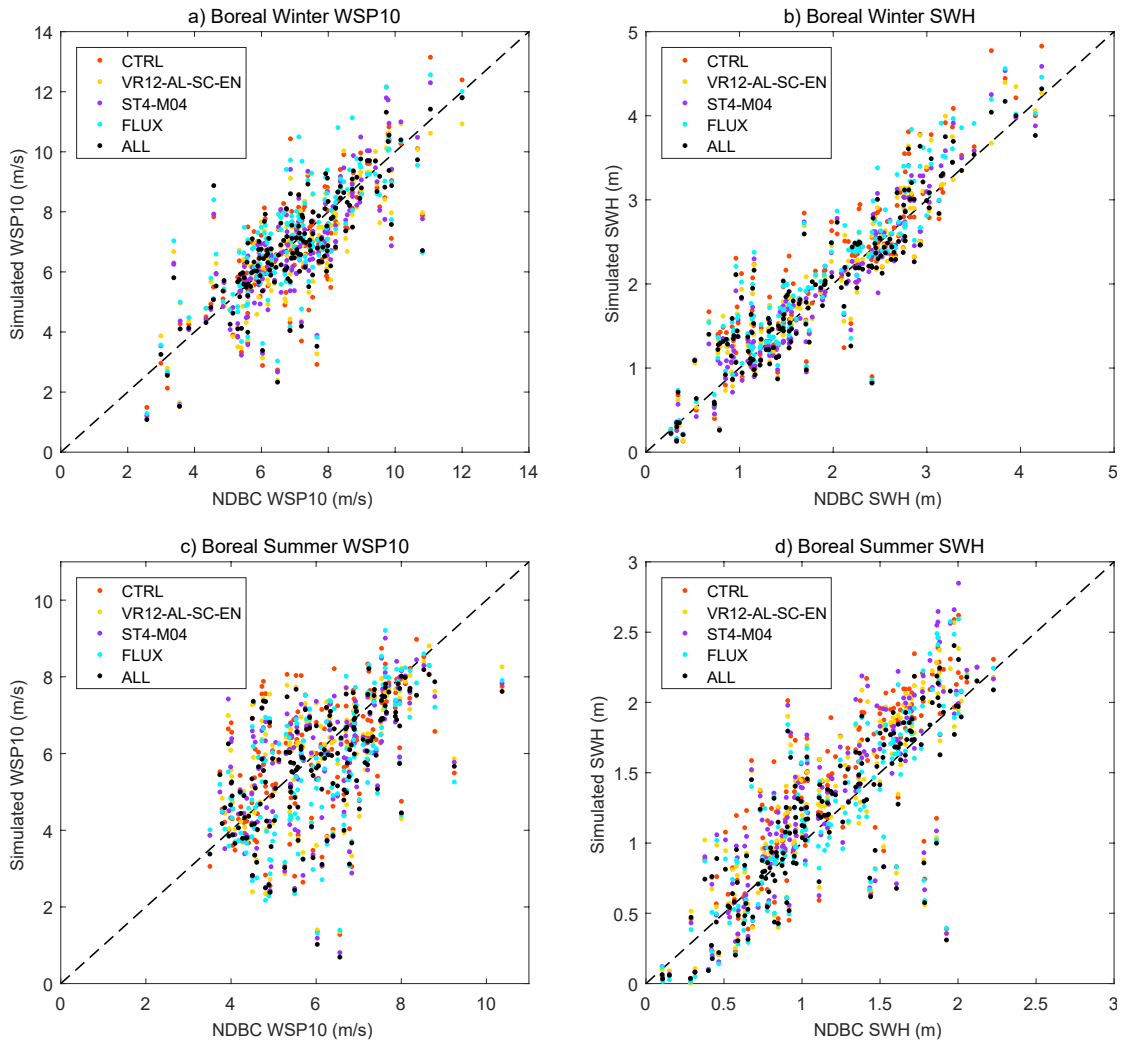

Figure 12. Scatter plots of simulated WSP10/SWH (y-axis) vs buoy WSP10/SWH (x-axis): (a) the WSP10 in Jan-Feb, 2017, (b) the SWH in Jan-Feb, 2017, (c) the WSP10 in Aug-Sep, 2018, and (d) the SWH in Aug-Sep, 2018. The dotted line is y=x. The corresponding mean biases with standard deviations and RMSEs for every experiment are shown in Table 2.